Characterisation of the Notch signalling small molecule inhibitor RIN1

Biljan, Ivica

Master's thesis / Diplomski rad

2023

Degree Grantor / Ustanova koja je dodijelila akademski / stručni stupanj: **University of Zagreb, Faculty of Science / Sveučilište u Zagrebu, Prirodoslovno-matematički fakultet**

Permanent link / Trajna poveznica: https://urn.nsk.hr/urn:nbn:hr:217:324487

Download date / Datum preuzimanja: **2024-05-10**

Repository / Repozitorij:

Repository of the Faculty of Science - University of Zagreb

University of Zagreb

Faculty of Science

Department of Biology

Ivica Biljan

Characterisation of the Notch signalling small molecule inhibitor RIN1

Master thesis

Zagreb, 2023.

Sveučilište u Zagrebu
Prirodoslovno-matematički fakultet
Biološki odsjek

Ivica Biljan

Karakterizacija malomolekulskog inhibitora RIN1 signalnog puta Notch

Diplomski rad

Zagreb, 2023.

Ovaj rad je izrađen u laboratoriju radne grupe AG Prof. Dr. Franz Oswald na Odjelu za Internu Medicinu I Sveučilišne Klinike Ulm, pod mentorstvom Prof. Dr. rer. nat. Franz Oswald, te komentorstvom Prof. Dr. Sc. Nada Oršolić. Rad je predan na ocjenu Biološkom odsjeku Prirodoslovno-matematičkog fakulteta Sveučilišta u Zagrebu radi stjecanja zvanja magistra eksperimentalne biologije (mag. biol. exp.).

Acknowledgements

I am immensely grateful to Prof. Dr. Franz Oswald for his expertise and guidance during my thesis supervision. Many thanks for the support, understanding and kindness that he showed throughout the entire time.

I also owe a huge debt of gratitude to Philipp Hoffmeister who was relentlessly there for my questions, especially for giving me the theoretical advice and pre-reviewing my thesis.

Thousand thanks to Sabine Schirmer who taught me how to carry out the experiments, especially many thanks for her incessant patience and indispensable wet lab tips and tricks she showed me.

Many thanks to Prof. Dr. Nada Orsolic for her invaluable support and kindness as a co-supervisor.

I am also tremendously grateful to Hina Zarrin, Min Guo, Qingwen Yang, Rosel Schmidt, Tim Schlosser and Tugba Demir for all the help, knowledge, support and kindness.

I would like to thank the entire lab for an absolutely amazing work climate, team work and care they showed :)

Last but not least, I am greatly indebted to my parents, sister and family for their selfless support and care.

Dedication

To I.C.,

with all my love

Sveučilište u Zagrebu
Prirodoslovno-matematički fakultet
Biološki odsjek   Diplomski rad

Karakterizacija malomolekulskog inhibitora RIN1 signalnog puta Notch

Ivica Biljan
Rooseveltov trg 6, 10000 Zagreb, Hrvatska

Notch signalni put je ključan u embrionalnom razvoju i homeostazi tkiva, sa središnjom dvojnom represorsko-aktivatorskom ulogom transkripcijskog faktora RBPJ. Aberantna signalizacija Notch puta doprinosi patogenezi mnogih bolesti te je posljedično važna meta terapijske inhibicije što se posebice odnosi na RBPJ na koji ciljano djeluju malomolekulski inhibitori poput RIN1 i CB-103. Kako bi se dobio detaljniji uvid u njihove molekularne mehanizme kao i *off-target* učinke, provedeni su luciferazni testovi na raznim kombinacijama transkripcijskih faktora. CB-103 doveo je do inhibicije samog enzima Firefly luciferaze, dok je RIN1 doveo do definitivne inhibicije Gal4 i HNF6 DNA vezanja. Nadalje, kako bi se analiziralo potencijalno izbacivanje ili inhibicija jezgrinog unosa RBPJ od strane inhibitora, proveden je test imunofluorescencije koji je pokazao da nema interferencije sa lokalizacijom RBPJ u jezgri. Posljednje, provedena je analiza obogaćenja genskih setova na javno dostupnim podacima RNA sekvenciranja iz T-stanične linije Jurkat tretirane inhibitorima kako bi se dobio uvid u detaljne genomske obrasce promjena ekspresije genskih setova. RIN1 i CB-103 pokazali su promjene u kontroli većeg broja genskih setova u usporedbi sa RBPJ *knock-down* djelovanjem siRBPJ te γ-sekretaznim inhibitorom DAPT što ukazuje na manje specifičan mehanizam djelovanja i/ili mnogo kompleksniju integraciju signalnih puteva nego što je trenutno poznato iz literature.

BASIC DOCUMENTATION CARD

University of Zagreb
Faculty of Science
Department of Biology   Master thesis

Characterisation of the Notch signalling small molecule inhibitor RIN1
Ivica Biljan
Rooseveltov trg 6, 10000 Zagreb, Croatia

The Notch pathway is essential for embryonic development and tissue homeostasis, with transcription factor RBPJ's central dual repressor/activator role. Aberrant Notch signaling contributes to the pathogenesis of many diseases and is consequently an important target of therapeutic inhibition which particularly pertains to RBPJ that is targeted by novel small molecule inhibitors like RIN1 and CB-103. To get more detailed insights into their molecular mechanisms and potential off-target effects, luciferase assays were performed on various transcription factor combinations. Firefly luciferase enzyme itself was inhibited by CB-103, while RIN1 conclusively inhibited only Gal4 and HNF6 DNA binding. Moreover, to analyze potential nuclear export or inhibition of nuclear import of RBPJ by inhibitors, immunofluorescence assay was performed which showed no interference with RBPJ's nuclear localization. Finally, Gene Set Enrichment Analysis was carried out on publicly available RNA sequencing data from inhibitor treated Jurkat T-cell line to get insights to in-depth genome-wide pattern in gene set expression changes. Both RIN1 and CB-103 exhibited changes in regulating a much higher number of gene sets compared to RBPJ knock-down by siRBPJ, and γ-secretase inhibitor DAPT, indicating less specific mode of action and/or more elaborate signal integration pathways than what is currently known from the literature.

Table of Contents

1. Introduction

1.1. Notch signaling pathway

Notch gene was first discovered at the beginning of 19th century in *Drosophila melanogaster* mutants that were heterozygous for *Notch* deficiency which led to notches on their wings. Complete deficiency of functional *Notch* gene was on the other hand lethal (Zhou *et al.*, 2022). It was later established that the Notch signaling is essential in metazoan organisms not only for embryonic development but also for tissue homeostasis throughout the entire lifespan (Lambris, 2018; D'assoro *et al.*, 2022). It is therefore not surprising that aberrant Notch signaling leads to a vast variety of diseases including genetic disorders e.g. Adams-Oliver syndrome, Alagille syndrome or Hajdu-Cheney syndrome (Mašek and Andersson, 2017), cardiovascular diseases e.g. cardiac arrythmia (De la Pompa and Epstein, 2012), kidney diseases e.g. focal segmental glomerulosclerosis (Mukherjee *et al.*, 2019) and numerous types of cancer e.g. leukemia, glioblastoma, melanoma and breast cancer (Lambris, 2018).

The canonical Notch signaling pathway (Figure 1.) is a direct cell-to-cell communication pathway that is initiated by physical contact between a ligand (in mammals- DELTA-LIKE 1, 3 and 4, JAGGED 1 and 2) and the Notch receptor (in mammals- NOTCH1 to NOTCH4) (Lambris, 2018). The mature Notch receptor consists of an extracellular domain (NECD), a transmembrane domain (TM) and the Notch intracellular domain (NICD). TM serves as a link between NECD which is a ligand-binding domain, and NICD which is a part of receptor that gets released and translocated into the nucleus upon ligand-induced S3 cleavage by γ-secretase (Fortini, 2002; Lambris, 2018). Apart from S3, there are also S1 and S2 cleavages. S1 cleavage which is involved in receptor maturation, takes place within Golgi apparatus and is exerted on glycosylated Notch precursors by furin-like protease (Zhou *et al.*, 2022). Ligand binding to Notch receptor and subsequent ligand endocytosis triggered by E3 ubiquitination of ligand's intracellular tail generates a pulling force on Notch receptor which exposes the S2 cleavage site (Ferreira and Aster, 2022). S2 cleavage is carried out by ADAM metalloprotease 10 and 17 and releases NECD while at the same time generating Notch extracellular truncation (NEXT). NEXT is then cleaved by γ-secretase to release NICD into the cytosol (Fortini, 2002; Lambris, 2018).

Upon its release into the cytosol, NICD is translocated into the nucleus where it binds to recombination signal binding protein for immunoglobulin kappa J (RBPJ) which is a DNA binding transcription factor (Jarriault *et al.*, 1995). The NICD-RBPJ complex then binds mastermind-like (MAML) co-activator leading to the formation of a ternary complex (Wu *et al.*, 2000) that eventually and in concert with other co-

activators like KAT2A and KAT2B activates transcription of Notch target genes. The main Notch target genes are members of *HES* and *HEY* family of proteins (Fischer and Gessler, 2007). The assembly of ternary complex is a stepwise process in which the RBPJ-associated module (RAM) domain of NICD binds to β-trefoil fold domain (BTD) of RBPJ which is followed by interaction between ankyrin repeats (ANK) of NICD and C terminal domain (CTD) of RBPJ. MAML binds at the end into the groove formed by ANK and CTD (Lambris, 2018).

In the absence of active Notch signaling, co-repressors such as SHARP/SPEN (Oswald *et al.*, 2002), KYOT2/FHL1 (Wang *et al.*, 2007) and histone H3K4 demethylase KDM5A bind to RBPJ which makes it the repressor of transcription (Lambris, 2018).

Activated Notch signaling comes to a halt when the Proline, Glutamic acid, Serine, Threonine (PEST) domain of NICD gets ubiquitinated by FBXW7 leading to its proteasomal degradation (Ferreira and Aster, 2022).
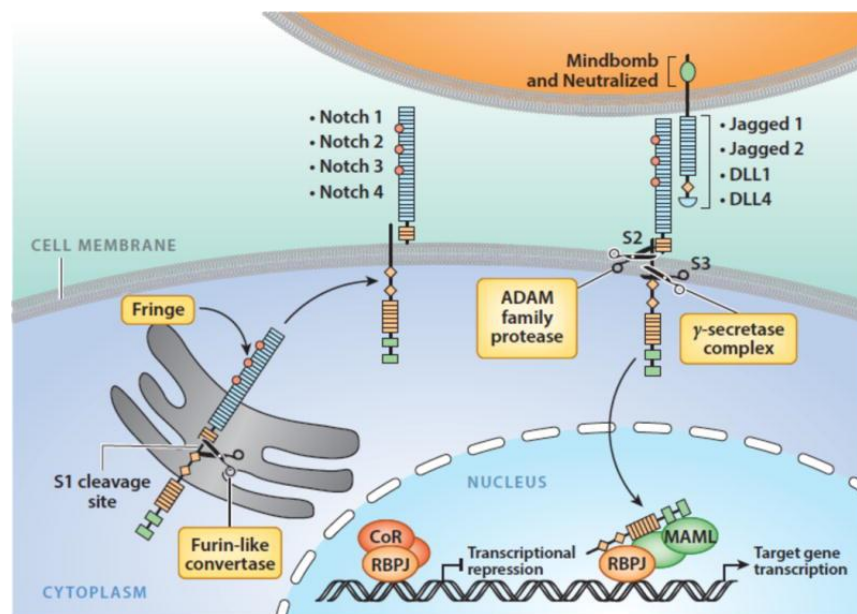
Figure 1. Overview of the Notch signaling pathway. Notch receptor precursors undergo the S1 cleavage by Furin-like convertase within the Golgi network. This is followed by glycosylation by Fringe enzyme leading to the formation of mature Notch receptors that are trafficked to and embedded into the cell membrane. Direct cell-to-cell contact is necessary to engage the Notch receptor (Notch1 to Notch4) by respective Notch ligand (Jagged 1, Jagged 2, DLL1, DLL4 and DLL3 (not shown in this figure)). Activation of Notch signaling leads to S2 and S3 cleavage steps by ADAM metalloprotease and γ-secretase complex, respectively. S3 cleavage releases the Notch intracellular domain which translocates into the nucleus and binds to transcription factor RBPJ displacing bound corepressors and leading to RBPJ's transcriptional switch from repressor into the activator. RBPJ-NICD complex then binds MAML and additional coactivators to induce transcription of Notch target genes. Figure taken from (Aster, Pear and Blacklow, 2017)

1.2. Notch signaling in cancer

Based on the sequencing of cancer genomes, Notch mutations can be classified into three main groups (Figure 2.) - mutations in the negative regulatory region (NRR) or NRR and PEST domain at the same time, mutations in PEST domain only, and mutations in other functional domains of Notch receptor. First two groups lead to gain of function mutations while the last one is responsible for the loss of function mutations (Ferreira and Aster, 2022).

In case of NRR mutations, Notch receptor is constitutively active as it is subjected to ligand-independent cleavage and generation of NICD. This is independent of tumor microenvironment (Aster, Pear and Blacklow, 2017; Ferreira and Aster, 2022). Most notable cancer examples of this case are T-cell acute lymphoblastic leukemia (T-ALL) (Weng *et al.*, 2004) and triple negative breast cancer (TNBC) (Ferreira and Aster, 2022). In T-ALL, NRR is most frequently disrupted by point mutations and indels, with NOTCH1 being the most common mutation found in more than 50% of T-ALL cases. However, although rarely, translocations are also possible and usually involve T-cell receptor β locus. On top of NRR mutations, T-ALL commonly exhibits PEST domain mutations that encompass non-sense or frameshift mutations (Weng *et al.*, 2004; Ferreira and Aster, 2022). As for TNBC, point mutations are rarely found. Instead, the oncogenic mechanism is based on gene rearrangements that result in the expression of constitutively active NOTCH1 and NOTCH2 receptors. This activation comes from the lack of NRR due to N-terminal truncation (Ferreira and Aster, 2022).

The effect of Notch mutations in the PEST domain only is dependent on tumor microenvironment as they still require ligand-dependent activation of Notch signaling. However, once the signaling has been activated, mutations interfere with the ubiquitin-dependent degradation of NICD leading to increased Notch signaling marked by its oncogenic role. This mutation pattern is characteristic of B cell tumors like chronic lymphocytic leukemia (CLL) (Fabbri *et al.*, 2011), splenic marginal zone lymphoma (SMZL) and diffuse large B cell lymphoma (DLBCL) (Lee *et al.*, 2009). In all three cancers, it is a matter of nonsense, frameshift or alternative splicing mutations (Ferreira and Aster, 2022).

The third group of mutations includes mutations in Notch receptor regions other than NRR and PEST domain which are the loss-of-function mutations as they impair the production of NICD and therefore Notch signaling. The mutated regions are commonly epidermal-growth-factor-like repeats (EGF) and ANK (Aster, Pear and Blacklow, 2017; Ferreira and Aster, 2022). Representative cancers are solid tumors like squamous cell carcinoma (SCC) (Wang *et al.*, 2011), bladder carcinoma (Rampias *et al.*, 2014) and glioma (The

Cancer Genome Atlas Research Network, 2015) which are caused by point substitutions, frameshift or nonsense mutations (Aster, Pear and Blacklow, 2017; Ferreira and Aster, 2022). Those mutations lead to either no expression of Notch receptors or expression of defective receptors with no intracellular signaling domain (Aster, Pear and Blacklow, 2017).
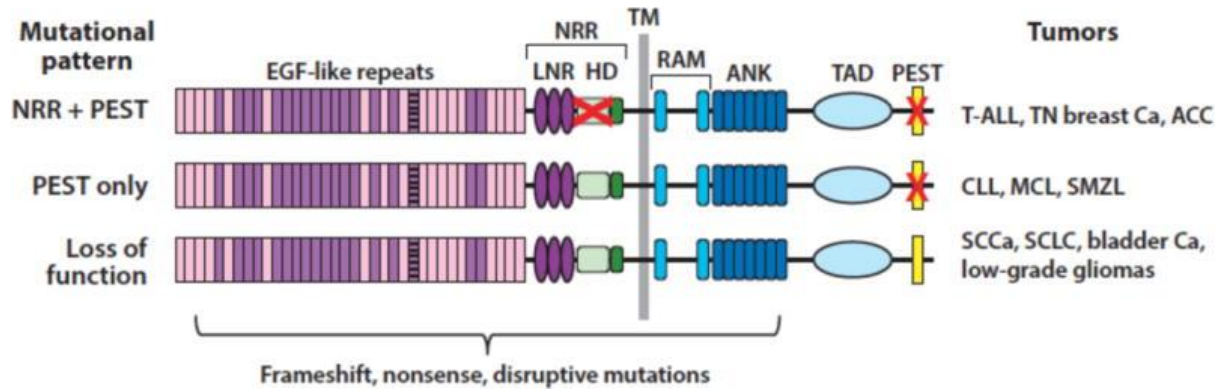
Figure 2. The three main patterns of Notch receptor mutations. The first pattern of Notch receptor mutations affects both the negative regulatory region (NRR) and Proline, Glutamic acid, Serine, Threonine (PEST) domain at the same time. It is present in T-cell acute lymphoblastic leukemia (T-ALL), triple negative breast cancer (TN breast Ca) and adenoid cystic carcinoma (ACC). The second mutational pattern comprises PEST domain only and is represented by chronic lymphocytic leukemia (CLL), mantle cell lymphoma (MCL) and splenic marginal zone lymphoma (SMZL). The third mutational pattern encompasses mutations in Notch receptor regions other than NRR and PEST domain that impair the production of NICD and consequently the Notch signaling. Commonly mutated regions in this case are epidermal growth-factor repeats (EGF-like repeats) and ankyrin repeats (ANK). Representative cancers are squamous cell carcinoma (SCC), small cell lung cancers (SCLC), bladder cancer (bladder Ca) and low-grade gliomas. Figure taken from (Aster, Pear and Blacklow, 2017)

1.3. Notch signaling as a therapeutic target

The main classes of potential Notch targeting drugs are S1, S2 and S3 cleavage inhibitors (γ-secretase inhibitors), monoclonal antibodies, antibody-drug conjugates and transcription blockers (Majumder *et al.*, 2021; Zhou *et al.*, 2022).

S1 cleavage inhibitors like CPA or CAD204520 target sarcoendoplasmic reticulum Ca^{2+} ATPase which is required for S1 Notch cleavage. However, there hadn't been any encouraging results in laboratory tests that would merit any clinical trials (Zhou *et al.*, 2022).

S2 cleavage performed by ADAM metalloprotease 10 or 17 is e.g. the target of dual ADAM10/17 inhibitor INCB7839 which is currently being tested in clinical trial (ClinicalTrials.gov Identifier: NCT04295759) for children with recurrent/progressive high-grade glioma.

The most studied small molecule Notch inhibitors are γ-secretase inhibitors that were initially developed to treat Alzheimer's disease since γ-secretase is responsible for amyloid precursor protein cleavage and the formation of β-amyloid peptide whose accumulation is one of the hallmarks of Alzheimer's disease (Majumder *et al.*, 2021; Luo and Li, 2022). Nevertheless, they failed clinical trials due to nonselective inhibition of substrates and massive side-effects such as infections, skin cancer and gastrointestinal distress like severe diarrhea (Majumder *et al.*, 2021; Luo and Li, 2022). Among the very few drugs to have reached phase III/IV clinical trials which are still ongoing at the time of writing this thesis, is PF-03084014 (ClinicalTrials.gov Identifier: NCT03785964) used in adult patients with desmoid tumor/aggressive fibromatosis (Zhou *et al.*, 2022).

To come around the limitations of γ-secretase inhibitors, other potential selective antibodies targeting different regions of different Notch receptors and ligands had been developed. For example, rovalpituzumab tesirine which is an antibody-drug conjugate targeting DLL3 showed promising results in initial studies of small-cell lung cancer and high-grade neuroendocrine tumors. Notwithstanding, the phase II and III trials failed to achieve required efficacy (Zhou *et al.*, 2022). Another monoclonal antibody against human *NOTCH1* called brontictuzumab underwent clinical trial for patients with solid tumors and lymphoid malignancies but failed to reach FDA approval (Zhou *et al.*, 2022; Wagner *et al.*, 2023). A monoclonal antibody against both *NOTCH2* and *NOTCH3*, OMP-59R5 (tarextumab), didn't show any benefits in first-line treatment of metastatic pancreatic ductal adenocarcinoma when used in combination with nab-paclitaxel and gemcitabine (Zhou *et al.*, 2022).

Transcription blockers primarily target the proteins downstream in the Notch signaling cascade, that is to say, the ternary complex (NICD, RBPJ and MAML). This remains largely unexplored with only a handful of examples such as RBPJ inhibitor 1 (RIN1) and CB-103, both of which target RBPJ (Hurtado *et al.*, 2019; Lehal *et al.*, 2020), and IMR-1 which is directed against MAML1 (Zhou *et al.*, 2022). Nevertheless, the first example of such kind was SAHM1- synthetic stapled α-helical peptide derived from MAML1. The peptide corresponds to Glu21 to Thr36 residues of MAML1 and is stapled to stabilize the helical structure which renders improved binding ability and metabolic stability. SAHM1 was shown to bind Notch 1 intracellular domain and competitively inhibit the binding of wild type MAML1 therefore repressing Notch1 target gene expression (Moellering *et al.*, 2009).

1.4. RBPJ-inhibitor 1 (RIN1)

Hurtado et al. (2019) developed a primary high-throughput screen to detect small molecules that could potentially target RBPJ. The screen was based on the interaction between RBPJ and SHARP which is a corepressor binding to the same RBPJ region as NICD. SHARP was fused to Gal4 DNA binding domain that binds to UAS sequence downstream of which is the luciferase gene. RBPJ was mutated so that it can't bind to DNA and was tagged with VP16. In case of interaction between SHARP and RBPJ, VP-16 induced transcription of luciferase gene, and led to emission of light, in transfected AD-293 cells. Compound library used for the primary screen had a concentration of single compounds at 10 µM. Secondary assay was then used to distinguish which compounds inhibit only RBPJ instead of SHARP. *NOTCH2* ICD was expressed in AD-293 cells that were transfected with *Hes1*-luciferase reporter. Newly discovered compound, RIN1 caused *Hes1*-luciferase inhibition with the half maximal inhibitory concentration of 0.18 µM. What is rather unusual and not clearly addressed in the study is the inhibition of RBPJ-VP16 construct which is supposed to induce transcription independently of NICD or any other coactivators. These results point out to either interference of RIN1 with RBPJ DNA binding, off-target inhibition of VP16 or inhibition of luciferase enzyme itself which will be addressed in my research project (Hurtado *et al.*, 2019).

Moreover, RIN1 was shown to decrease proliferation of three cancer cell lines such as Jurkat (T cell leukemia), Kopt-K1(Precursor T-cell acute lymphoblastic leukemia) and Rec-1 (Mantle cell lymphoma) characterized by activating *NOTCH1* mutations. Nevertheless, the inhibitory effect was dependent on the cell line indicating context-dependent differences in inhibition (Hurtado *et al.*, 2019).

To gain a better mechanistic insight into the mode of action of RIN1 and compare it to other known compounds, RNA sequencing was carried out on Jurkat cells treated with 2 µM RIN1, 2 µM DAPT and 10 µM CB-103, as well as siRNA against RBPJ. Gene clustering was then performed on genes that were differentially expressed with a fold change higher than 2 and $p<0.05$ and that at the same time didn't significantly differ between negative control groups which are DMSO for all small molecule inhibitors and control siRNA for siRNA against RBPJ (fold change less than 1.4 and $p< 0.05$). Only a handful of genes satisfied this requirement and they were later confirmed by qRT-PCR. Some notable ones include *HES1, HEY1* and *DTX*. CB-103 clustered together with DAPT which is a γ-secretase inhibitor indicating that the mechanism of action might be at the level of upstream Notch receptor. This is however still elusive as the other study presented hereinafter came to a different conclusion. RIN1 on the other hand clustered with siRNA against RBPJ suggesting that it acts downstream at the level of RBPJ (Hurtado et al., 2019).

1.5.   CB-103

Notch inhibitor 6-(4-(tert-butyl)phenoxy)pyridine-3-amine shortly known as CB-103 was discovered in a high throughput screen consisting of 'signal-sending' HeLa cells expressing Delta-like 4 ligand (DLL4) and 'signal-receiving' HeLa cells expressing *NOTCH1* receptor and harboring a luciferase gene under the 12x RBPJ binding site. CB-103 led to the inhibition of Notch signaling and therefore luciferase activity both in initial screen with *NOTCH1* but also in additional assays with all the other mammalian Notch receptors (Lehal *et al.*, 2020).

In addition, it was shown that CB-103 inhibited the growth of two T cell acute lymphoblastic leukemia cell lines, namely T-ALL1 and RPMI-8402, characterized by increased Notch activation. In this case, CB-103 downregulated the expression of *NOTCH1* and Notch target genes *DTX1, MYC* and *HES1* (Lehal *et al.*, 2020).

The same study later identified G193R mutation in RPMI-8402 T-ALL cell line resistant to CB-103 activity. This mutation is harbored within the BTD (β-trefoil fold domain) of RBPJ and its role in CB-103 insensitivity was confirmed by molecular docking studies. The same pocket within BTD of RBPJ within which CB-103 binds, is the binding site for RAM domain of NICD which is the molecular basis of Notch transcription complex inhibition. Chromatin immunoprecipitation experiments also confirmed the proposed mode of action. Namely, CB-103 led to no recovery of Notch1 ICD in case of V5-tagged wild type RBPJ but the band was clearly visible on Western blot from V5-RBPJ G193R mutant (Lehal *et al.*, 2020).

2. Study aims

The Notch signaling pathway is a highly conserved signaling pathway requiring the physical interaction between a DSL ligand and Notch receptor on two neighboring cells. It is important for embryonic development and tissue homeostasis and therefore, its dysregulation is involved in a variety of human diseases, most notably cancer. Consequently, Notch signaling has been a target of therapeutic inhibition. The novel class of inhibitors are transcription blockers such as RIN1 and CB-103 which target the NICD-RBPJ-MAML ternary complex. However, their molecular mechanism of inhibition is not yet clear.

Therefore, the aims of this study are:

1. To characterize RIN1 and CB-103 in terms of the molecular mechanisms of their action in a series of luciferase assays performed on various transcription factor combinations
2. To analyze a potential nuclear export or inhibition of nuclear import of RBPJ by RIN1 and CB-103 using immunofluorescence microscopy
3. To characterize the broader impact and potential off-target effects of RIN1 and CB-103 within the entire cellular context by applying Gene Set Enrichment Analysis on publicly available RNA sequencing data from inhibitor treated Jurkat T-cell line (NCBI GEO Accession number GSE134401).

3. Materials

During the preparation of the practical part of my thesis, I used the following materials:

3.1. Chemicals, substances and reagents

DMEM with GlutaMAX supplement	Thermo Fisher Scientific (Waltham, Massachusetts, USA)
DMSO	Sigma-Aldrich Chemie GmbH, (Steinheim)
Ethanol	Sigma-Aldrich Chemie GmbH, (Steinheim)
FCS (Fetal Calf Serum)	Biochrom GmbH (Berlin)
Lipofectamine2000®	Thermo Fisher Scientific (Waltham, Massachusetts, USA)
Opti-MEM I Reduced Serum Medium	Thermo Fisher Scientific (Waltham, Massachusetts, USA)
PBS	Thermo Fischer Scientific (Darmstadt)
Penicillin/streptomycin	Thermo Fischer Scientific (Darmstadt)
PFA (4% in PBS)	Merck KGaA (Darmstadt)
Trypan blue	Sigma-Aldrich Chemie GmbH (Steinheim)

3.2. Consumable materials

96-well microplate (pureGrade™, black, U-bottom)	BRAND GmbH + CO KG (Wertheim, Germany)
Cell culture dish (Greiner CELLSTAR® dish, diam. × H 100 mm × 20 mm, vented)	Greiner Bio-One GmbH (Frickenhausen, Germany)
Cell culture plate (Greiner CELLSTAR® multiwell culture plates, 48 wells (TC treated with lid))	Greiner Bio-One GmbH (Frickenhausen, Germany)

Cover slip	Carl Roth GmbH & Co. KG (Karlsruhe, Germany)
Falcon® round bottom polystyrene tube (5 mL)	Corning Science (Kaiserslautern)
Falcon® conical centrifuge tube polypropylene (15/50mL)	Corning Science (Kaiserslautern)
Glass Pasteur Pipettes	Brand GmbH + CO KG (Wertheim, Germany)
Microscope slide	VWR International GmbH (Darmstadt, Germany)
Pipette tip (10/20/200/1000 µL)	Carl Roth GmbH & Co. KG (Karlsruhe)
Pipette tip for Multipette (125 mL)	Carl Roth GmbH & Co. KG (Karlsruhe)
Reaction tube (1.5 mL)	Carl Roth GmbH & Co. KG (Karlsruhe)
Serological pipette (1/2/5/10/25 mL)	Corning Science (Kaiserslautern)

3.3. Devices and equipment

Analytical balance CP423S	Sartorius AG (Göttingen, Germany)
Eppendorf 5417R Refrigerated Centrifuge	Eppendorf AG (Hamburg, Germany)
Fluorescence Inverted System Microscope IX71	Olympus Europa SE & Co. KG (Hamburg, Germany)
Heidolph Polymax 1040 Wave Platform Shaker	Heidolph Instruments GmbH & CO. KG (Schwabach, Germany)
Heidolph REAX 2000 Vortex Mixer	Heidolph Instruments GmbH & CO. KG (Schwabach, Germany)
Incubator HERAcell 150	Kendro Laboratory Products GmbH (Hanau,Germany)

Microplate Luminometer Centro LB960	BERTHOLD TECHNOLOGIES GmbH & Co. KG (Bad Wildbad, Germany)
Multipette® M4 - Multi-Dispenser Pipette	Eppendorf SE (Hamburg)
Neubauer Counting Chamber	Marienfeld superior GmbH (Lauda-Königshofen)
Pipetus	Hirschmann Laborgeräte GmbH & Co. KG (Eberstadt, Germany)
Suction pump Mini-Vac ECO	PeqLab Biotechnologie (Erlangen)
Thermo Scientific Multifuge 1S Centrifuge	Thermo Fischer Scientific (Darmstadt)
Water Bath E100	LAUDA GmbH & Co. KG (Lauda-Königshofen)
Zeiss Axiovert 25 Inverted Phase Contrast Microscope	Carl Zeiss AG (Oberkochen)

3.4.   Software

Adobe Illustrator 2020	Adobe Inc. (San José, California, USA)
GraphPad Prism 9	GraphPad (San Diego, USA)
ImageJ 1.53t	National Institutes of Health (Bethesda, Maryland, USA)
MikroWin2000	Mikrotek Laborsysteme GmbH (Overath, Germany)
GSEA v. 4.3.2.	Broad Institute, UC San Diego
Cytoscape v. 3.9.1.	cytoscape.org.(Multiple partner organisations and institutes)
Mendeley Reference Manager v. 2.80.1	Mendeley Ltd. (Elsevier)

3.5. Cell lines

HeLa

HeLa wt	human cervical cancer cell line
HeLa RBPJ KO#42	human cervical cancer cell line with CRISPR-Cas9 induced RBPJ knockout (Wolf *et al.*, 2019)

3.6. Inhibitors

RIN1	Selleckchem (Selleck Chemicals GmBbH, Planegg, Germany)
CB-103	MedChemExpress (Monmouth, USA)

3.7. Antibodies

Immunofluorescence

Primary antibody/species	Manufacturer
Monoclonal Anti-RBP-Jκ 1F1 (IgG2)/ rat	Merck Millipore (Burlington, MA, USA)

Secondary antibody/species	
Anti-Rat IgG (H+L) Alexa Fluor® 488/goat	Thermo Fisher Scientific (Waltham, Massachusetts, USA)

3.8. Plasmids

All full plasmid names are written as appearing in AG Oswald's clone chart. 3xκB luc and RelA are a courtesy of PD Dr. Bernd Baumann, University of Ulm.

Full name	Abbreviation
pGa981-6	pGa981-6
pcDNA3.1(-)hsNICD-EHEB	NICD-EHEB
pcDNA3.1-Flag2-mRBPJ-CRr(wt)	RBPJ wt
pcDNA3.1-Flag-mRBPJ-Cr-VP16(wt)	RBPJ-VP16

pcDNA3.1-Flag-mRBPJ-Cr-VP16(F261A/L388A)	RBPJ-VP16-DM
pcDNA3.1-Flag-mRBPJ-Cr-VP16-NBM(E398R/ F261A/V263A/R422E/E425R)	RBPJ-VP16-NBM
pFR-Luc	pFr-Luc
pcDNA3-Gal4-VP16-1	Gal4-VP16
pRL-TK(Renilla)	pRL-TK
pGL3-Basic	pGl3 basic
pGL3-Control	pGl3 control
Gal4-p65	Gal4-p65
3xκB luc	3xNFkB luciferase
RelA	p65 (RelA)
phsHNF6-Luc	HNF6- Luc
pcDNA3-VP16-HNF6wt	HNF6-VP16
pcDNA3-Flag1-HNF6wt	HNF6wt

4. Methods

4.1. HeLa (wt and RBPJ KO#42) cell culture

I cultured HeLa wild type and RBPJ KO#42 (CRISPR-Cas9 induced RBPJ knockout) cells in Dulbecco's Modified Eagle Medium (DMEM) with addition of 10% FCS and 1% penicillin/streptomycin antibiotics. Depending on when the cells had to be used for an experiment, I seeded different amounts given below in a total volume of 10 mL medium in 10 cm 1 compartment cell culture dish:

Mon to Fri- 0.2 million	
Mon to Wed- 0.5 million	
Fri to Mon- 0.3 million	
Fri to Tue- 0.2 million	
Wed to Fri- 0.5 million	

Naming convention explanation:

Mon to Fri- 0.2 million means seeding cells on Monday to use them on Friday- 0.2 million cells in 10 mL medium

I washed seeded cells with 5 mL PBS, and trypsinized with 2 mL trypsin for a duration of 3 min at 37 °C in the incubator (6% CO_2, 95% relative air humidity). I inactivated trypsin by putting those 2 mL of trypsinized cell suspension in 8 mL DMEM medium. I took an aliquot of cells into a 1.5 mL Eppendorf tube, which I subsequently mixed with trypan blue in a 1:1 ratio (50 µL of cell suspension and 50 µL of trypan blue) to stain dead cells in the follow-up cell count using a Neubauer chamber. To count cells for maintaining them in the culture, I used 2 of the large squares in the corner of the 9-square-grid, each containing 16 smaller squares. To seed the cells for conducting experiments, I used all 4 corner squares for counting.

4.2.   Lipofectamine2000™ transfection

General version of the protocol is given below and the plasmids used for transfection together with respective amounts are given in the results section.

I prepared two transfection mixes: 'DNA mix' and 'Lipofectamine mix'. I prepared each mix in 5 mL round bottom polystyrene test tubes, and each of them corresponding to two wells on a 48-well plate (24 test tubes in total for one 48-well plate). I prepared the first mix by putting 50 µL of Opti Minimal Essential Medium (Opti-MEM) I Reduced Serum Medium into the tube which I followed by successive addition of required plasmid DNA volumes as calculated from the desired amount of DNA to be used for transfection. I then vortexed all 'plasmid DNA' mixes. The second mix consisted of 50 µL Opti-MEM medium and of 2 µL Lipofectamine2000™ Transfection Reagent. I vortexed all 'lipofectamine' mixes. Afterwards, I added the 'plasmid DNA' mix to the 'lipofectamine2000' mix and immediately vortexed which I followed by incubation at room temperature for 5 min. I then again shortly vortexed before adding the final mix containing plasmid DNA within lipofectamine vesicles to the cells by putting 50 µL of the mix to one well

and 50 µL to the other, slowly in a dropwise manner by evenly distributing the mix over the well. I incubated the cells for 24 hours at 37 °C in an incubator (6% CO_2 and 95% relative air humidity) prior to harvesting.

4.3.   Inhibitor treatment

4.3.1.   HeLa RBPJ KO#42- luciferase assay

Five hours post transfection, I treated the cells with RIN1 and CB103 inhibitors. Used concentrations were: 2.5 µM, 5 µM and 10 µM for RIN1; and 10 µM, 20 µM and 40 µM for CB103. I prediluted both inhibitors in DMSO before applying them to cells in equal volume of 1µL which allows the use of single 1/500 DMSO dilution as a solvent control. For RIN1, solutions with concentrations of 1.25 mM, 2.5 mM and 5 mM were prepared, while for CB103 concentrations of 5 mM, 10 mM and 20 mM were used. Adding 1 µL of each solution to 500 µL of cell solution led to the above stated concentrations. With respect to DMSO, I applied 1 µL of pure 100% DMSO. I applied each chosen inhibitor concentration to 6 wells of a 48-well plate (all treatment conditions performed in sextuplets). Moreover, to make it easier to pipette the required inhibitor volumes and increase the accuracy, I prediluted all inhibitor volumes of 1 µL 1:10 in DMEM (10% FCS, 1% penicillin/streptomycin) but in bulks (7 µL of inhibitor stock + 63 µL of DMEM) and applied 10 µL thereof to each well.

4.3.2.   HeLa wt- immunofluorescence

I treated the cells with respective inhibitor concentrations as indicated in the Table 1. below which also lists antibodies used in each of the square chambers during immunofluorescence experiment. Please refer to Immunofluorescence section of methods part for further details on the actual experiment.

Table 1. The immunofluorescence experimental setup[a]

1 HeLa wt RIN1 10 μM Anti-RBP-Jκ Anti-rat Alexa Fluor® 488	**2** HeLa wt RIN1 2.5μM Anti-RBP-Jκ Anti-rat Alexa Fluor® 488	**3** HeLa wt CB103 40 μM Anti-RBP-Jκ Anti-rat Alexa Fluor® 488
8 HeLa RBPJ KO#42 Untreated Anti-RBP-Jκ Anti-rat Alexa Fluor® 488	**NOT IN USE**	**4** HeLa wt CB103 10μM Anti-RBP-Jκ Anti-rat Alexa Fluor® 488
7 HeLa wt Untreated Anti-rat Alexa Fluor® 488	**6** HeLa wt Untreated Anti-RBP-Jκ Anti-rat Alexa Fluor® 488	**5** HeLa wt DMSO 1/500 Anti-RBP-Jκ Anti-rat Alexa Fluor® 488

[a]Squares represent the chambers of a 25 chamber square Petri dish. For simplicity, the outermost row of chambers is not shown. 55,000 HeLa wild type cells were seeded into each chamber and treated with respective amounts of inhibitors as shown above. The primary antibody used was Anti-RBP-Jk while the secondary one was Anti-rat Alexa Fluor® 488.

4.4. Luciferase assay

4.4.1. Single reporter firefly luciferase assay system

The luciferase assay is used to investigate if a protein of interest can bind to a promoter of a target gene and therefore activate the expression of the downstream located luciferase gene. Cells are usually co-transfected with expression plasmids for the protein of interest whose transcriptional activity is supposed to be determined and the specific luciferase reporter plasmid. They are then lysed, frozen overnight and luciferase substrate- D-luciferin is added which in the presence of enzyme, together with ATP and Mg^{++} ions , gets oxidized into a fluorescent product whose intensity of emitted light can be measured with a luminometer (Carter et al., 2015.; Smale, 2010).

16

The experiment was performed during 4 days and was conducted in the following stages:

a) Cell seeding into 48-well plate

I seeded 20,000 HeLa RBPJ KO#42 cells in 0.5 mL DMEM (10% FCS, 1% penicillin/streptomycin) per well onto 48-well plate.

b) Lipofectamine2000™ transfection

Exactly, 24 hours after seeding, I transfected the cells with lipofectamine2000™ as described in section 4.2.

c) Inhibitor treatment

Five hours post transfection, I treated the cells with inhibitors as described in section 4.3.1.

d) Cell harvesting

I harvested the cells 24 hours after transfection. I washed them with 1.5 mL PBS and subsequently lysed with 100 µL lysis reagent (Promega 5x cell culture lysis reagent diluted 1:5 with autoclaved distilled water). Lysis incubation time was 25 min at RT on a 3D rocking motion platform shaker. I transferred the lysates to 1.5 mL Eppendorf tubes and froze them overnight (or for several days) at -20 °C prior to proceeding with luminometer measurement.

e) Luminometer measurement

I thawed the lysates and subsequently centrifuged them for 4 min at 4 °C and 14,000 rpm. I transferred 80 µL of the supernatant into a new 1.5 mL Eppendorf tube. I prepared the Luciferase reagent by pipetting 10 mL of Luciferase assay buffer into the lyophilized luciferase assay substrate vial. I stored the solution at -80 °C and thawed it prior to subsequent measurements. I transferred 10 µL of each lysate into the well of a 96-well plate, which I loaded into the luminescence microplate reader Centro LB960. Measurement settings in Mikrowin 2000 software were:

1. Dispense
   a. Injector: 2
   b. Volume: 50 µL
   c. Speed: low
   d. Measurement operation: by well
   e. Repeated operation: Yes
2. Shake
   a. Duration: 2 sec
   b. Speed: normal
   c. Diameter: 1.0 mm
   d. Type: linear
   e. Measurement operation: by well
   f. Repeated operation: Yes
3. Delay
   a. Duration: 2.0 sec
   b. Measurement operation: by well
   c. Repeated operation: Yes
4. Firefly
   a. Name: Firefly
   b. Counting time: 10 sec
   c. Measurement operation: by well

4.4.2. Dual luciferase reporter assay system- *Firefly* and *Renilla*

Dual luciferase assay was carried out using the protocol from official Promega's technical manual: 'Dual-Luciferase Reporter Assay System', instructions for use of products E1910 and E1960, Revised 6/15 TM040 (Promega, 2015) and the core protocol from AG Oswald's research group.

Firefly and Renilla luciferase enzymes belong to different species, the former one being isolated from the North American firefly *Photinus pyralis*, and the latter produced by *Renilla reniformis* also known by the common name of Sea pansy and belonging to taxonomical group of cnidarians. Due to their different evolutionary origin, they have 'dissimilar enzyme structures and substrate requirements' which allows the use of Dual Luciferase Reporter (DLR) assay system. DLR assay system is based on two sequential reactions. First, beetle luciferin is oxidized by firefly luciferase in the presence of ATP and Mg^{2+} to generate oxyluciferin and a flash of light that is measured by a luminometer, which is followed by addition of patented Stop & Glo Reagent that quenches firefly luciferase and activates Renilla luciferase that oxidizes coelenterate-luciferin (coelenterazine) to coelenteramide along with a generation of a flash of light. Another major difference in procedure compared to the single reporter Firefly luciferase assay is the use of Passive Lysis Buffer that minimizes background luminescence of coelenterazine making it especially suitable for subsequent data analysis (Promega Corporation (Instructions for use of Products E1910 and E1960), 2015).

Dual luciferase reporter system has an advantage of controlling for sample-to-sample variability that arises from different transfection efficiency. *Renilla* luciferase is used as an internal control and the absolute luminescence value of *Firefly* luciferase is then normalized to that of *Renilla*.

Dual luciferase reporter assay system experiment was also performed during 4 days and was conducted in the following stages (for a) to c), please refer to the single reporter Firefly luciferase assay system):

a)   Cell seeding into 48-well plate
b)   Lipofectamine2000™ transfection
c)   Inhibitor treatment
d)   Cell harvesting

I harvested the cells 24 h after transfection. I washed them with 1.5 mL PBS and subsequently lysed with 75 µL of passive lysis buffer (Promega 5x Passive Lysis Buffer diluted 1:5 with autoclaved distilled water). Lysis incubation time was 15 min at RT on a 3D rocking motion platform shaker. I transferred the lysates to 1.5 mL Eppendorf tubes and froze them overnight (or for several days) at -20 °C prior to proceeding with luminometer measurement.

e)   Luminometer measurement

I thawed the lysates and centrifuged them for 4 min at 4 °C and 14,000 rpm. I transferred 55 µL of supernatant into new 1.5 mL Eppendorf tubes. I prepared the Luciferase Assay Reagent II (LAR II) by resuspending lyophilized Luciferase Assay Substrate with 10 mL of Luciferase Assay Buffer II which was subsequently stored at -80 °C. I prepared Stop & Glo Reagent by diluting 50x Stop & Glo Substrate in the required amount of Stop and Glo Buffer to a final concentration of 1x. I transferred 20 µL of each lysate into a well of a 96-well plate, which I subsequently loaded into the luminescence microplate reader. Measurement settings in Mikrowin 2000 software were:

1) Dispense
    a. Injector: 2
    b. Volume: 100 µL
    c. Speed: middle
    d. Measurement operation: by Well
    e. Repeated operation: Yes
2) Delay
    a. Duration: 2 sec
    b. Measurement operation: by Well
    c. Repeated operation: Yes
3) Firefly
    a. Name: Firefly
    b. Counting time: 10 sec
    c. Measurement operation: by well

4) Dispense
    a. Injector: 3
    b. Volume: 100 µL
    c. Speed: middle
    d. Measurement operation: by Well
    e. Repeated operation: Yes
5) Delay
    a. Duration: 2 sec
    b. Measurement operation: by Well
    c. Repeated operation: Yes
6) Renilla
    a. Name: Renilla
    b. Counting time: 10 sec
    c. Measurement operation: by well

4.5. Immunofluorescence

Immunofluorescence is a method that utilizes antigen-antibody complexes, whereby antibody is conjugated to either a fluorochrome or chromogenic enzyme, to visualize the expression of a protein of interest. If the protein of interest is an intracellular one, after initial preparation of the sample (fixation, inactivation of fixating agent and cell membrane permeabilization), the sample is incubated with a primary antibody specific to the antigen present on the protein of interest. This is followed up by addition of the secondary antibody recognizing the Fc region of the primary one. The secondary antibody is conjugated with a fluorochrome or chromogenic enzyme which allows visualization of the protein of interest under the fluorescence microscope.

Immunofluorescence method in my case consisted of three main steps:

a) Cell seeding

I seeded 55,000 HeLa wt cells in 1 mL of 10% FCS and 1% penicillin/streptomycin DMEM medium per chamber into a 100 mm square Petri dish with 25 compartments. I used only the inner 8 compartments forming a rectangle. Prior to seeding, I flamed coverslips and placed them into each chamber which I then coated with 500 µL fibronectin. I prepared the fibronectin solution by adding 900 µL PBS to 100 µL 10x

20

fibronectin solution. I incubated the fibronectin coated chamber dish for 30 min at 37 °C in the incubator (6% CO_2 and 95% air humidity) and then washed twice with PBS before seeding with cells in a manner indicated above.

b) Inhibitor treatment

Exactly, 24 hours after seeding, I treated the cells with respective inhibitor concentrations as indicated in the inhibitor treatment section 4.3.2. hereinabove.

c) Immunofluorescence

I performed the actual immunofluorescence procedure 24 hours after inhibitor treatment. I sucked out the medium from chambers and washed the cells once with 1 mL PBS. I followed it by fixation with 1 mL of 4% paraformaldehyde (PFA) in PBS for 20 min at RT on a shaker. I removed PFA using a pipette and collected it as waste into a separate 50 mL Falcon tube. Subsequently, I washed the cells twice with 1 mL PBS. In order to inactivate the PFA, I applied 1 mL of 50 mM ammonium chloride in PBS to the chambers, which I incubated for 10 min at RT on the shaker. I sucked out ammonium chloride with vacuum pump and washed the cells twice with 1 mL PBS. Afterwards, I put 1 mL of 0.2% Triton in PBS onto the cells for permeabilization which was carried out for 2 min at RT on a shaker. I sucked Triton out using a vacuum pump and washed the cells twice with 1 mL PBS. I blocked the unspecific antibody binding with 1 mL blocking buffer (1% BSA, 1% FCS and 0.1% Fish skin gelatin), which I incubated for 30 min at RT on a shaker. I removed the blocking buffer using a vacuum pump. All subsequent steps were performed in the dark. I added 350 µL of primary antibody (anti-RBP-Jκ clone 1F1 diluted 1:250 with blocking buffer) to each chamber and incubated for 3 hours at RT on a shaker. I sucked out the primary antibody using the vacuum pump and subsequently washed the cells three times with 1mL PBS. For each washing step, I incubated the cells for 5 min at RT on the shaker. I added 1 mL of secondary antibody (anti-rat Alexa Fluor 488 diluted 1:1000 with blocking buffer) to each chamber and incubated for 1 hour at RT on a shaker. 30 min after the incubation time with the secondary antibody, I added 1:800 diluted DAPI solution (1.25 µL of stock c= 5mg/mL DAPI) to the cells. After the incubation had been completed, I sucked out the secondary antibody and DAPI using the vacuum pump and washed the cells 6 times with 1mL PBS, each time incubating for 5 min at RT on a shaker. I took the coverslips with cells out of the square petri dish and turned them upside down before putting them onto the mounting medium, which I placed on the microscope slides. I stored the samples overnight in the dark in the cold room at 4 °C prior to observing them under the fluorescence microscope.

Fluorescence images were taken using Fluorescence Inverted System Olympus Microscope IX71 equipped with a digital camera (Hamamatsu C4742-95) and a 100 W mercury lamp (Osram, HBO 103W/2). Filter set used for RBPJ detection was ex: HQ480/40, em: HQ535/50. Filter set used for DAPI detection was ex: D360/50, em: D460/50

4.6. Gene Set Enrichment Analysis (GSEA), leading-edge analysis and generation of enrichment maps in Cytoscape

'Gene Set Enrichment Analysis is a computational method that determines whether an *a priori* defined set of genes (based on published information about biochemical pathways or co-expression in previous experiments) shows statistically significant, concordant differences between two biological states' (*https://www.gsea-msigdb.org/gsea/doc/GSEAUserGuideFrame.html*, no date; Subramanian *et al.*, 2005). Gene sets are on the other hand defined as 'groups of genes that share common biological function, chromosomal location or regulation' (Subramanian *et al.*, 2005).

GSEA's algorithm works by first ranking the genes based on e.g. their calculated differential expression values regardless of a gene set they belong to. This gives a list L of all genes of interest whose differential expression was calculated from e.g. microarray or RNA sequencing data. GSEA then determines whether the members of the *a priori* defined set of genes S from a curated gene database (e.g. Molecular Signatures Database), which are grouped based on their biological function, chromosomal location or regulation, are 'randomly distributed throughout the list L or primarily found at the top or bottom'. If the genes from a certain gene set are linked to the observed phenotype, they tend to cluster at either top or bottom of the list. The unit of measurement of how much the *a priori* gene set S is clustered at either the top or bottom of the ranked gene list L is the enrichment score (ES). To calculate the ES, algorithm walks down the ranked list of genes L and increases a running-sum statistic each time it encounters the gene that belongs to the same *a priori* defined gene set S. In the same way, it decreases the statistic if it encounters the genes that do not belong to the same gene set S. The magnitude of increase or decrease is proportionate to the correlation of gene with the phenotype whereby most and least correlated genes are present at the top or bottom of the list, respectively. 'The actual ES is the maximum deviation from zero encountered in the random walk; it corresponds to a weighted Kolmogorov–Smirnov-like statistic' (Subramanian *et al.*, 2005).

In case of a statistically significant ES for a given *a priori* gene set S, not all genes belonging to the given set S are necessarily highly contributing to the ES. Those that give the highest contribution to the ES are those that account for the core enrichment and are called the leading-edge subset. They appear 'at or before the point where the running sum reaches its maximum deviation from zero' and are a matter of leading-edge analysis (Subramanian *et al.*, 2005).

While performing the Gene Set Enrichment Analysis, given pathway enrichment information is often redundant because multiple genes are usually involved in multiple pathways and so the enrichment results can represent several versions of the same pathway. To come around this problem, the enrichment maps which can show overlaps between different pathways are used. The enrichment map is a network consisting of two elements which are the nodes and edges. Nodes represent gene sets while edges correspond to overlaps between the respective gene sets. Node size is proportionate to the number of genes in the gene set and edge thickness to the number of genes that overlap. Gene sets with high overlaps are additionally put together into clusters. Each node has a certain color on a color gradient that is proportionate to the value of enrichment score and details are provided in the color legend of the software.

To carry out GSEA and follow it up with leading-edge analysis and generation of enrichment maps, I first downloaded the Java-based software packages with graphical user interface from their official websites. I downloaded GSEA from the University of California, San Diego, Broad Institute's website- https://www.gsea-msigdb.org/gsea/index.jsp and Cytoscape from https://cytoscape.org/ . After downloading Cytoscape, I installed the Enrichment Map plug-in used to generate the enrichment maps.

The data I used for GSEA analysis are publicly available RNA sequencing data from (Hurtado *et al.*, 2019) . The data are from a Jurkat T-cell line treated with 2 µM RIN1, 2 µM DAPT and 10 µM CB-103, as well as siRNA against RBPJ (100 µL cells at 20 million cells/mL and 100 µL siRNA at 100 µM). I went to the National Center for Biotechnology Information's Gene Expression Omnibus (NCBI GEO) website (https://www.ncbi.nlm.nih.gov/geo/) and used the accession number GSE134401 to retrieve the following supplementary files 'GSE134401_CB-103_10uM_vs_DMSO.txt.gz ; GSE134401_DAPT_vs_DMSO.txt.gz ; GSE134401_RIN1_2uM_vs_DMSO.txt.gz and GSE134401_siRBPJ_vs_siCTRL.txt.gz. Those files contain the results from the final data processing step of RNA sequencing analysis.

Text files of results were extracted from .gz archive using WinRAR software (https://www.win-rar.com/start.html?&L=0). A preview of the data contained within the text files is given in the Table 2. below for 'GSE134401_DAPT_vs_DMSO.txt' file. Text file was opened in Microsoft Excel program.

Table 2. The preview of differential expression data for DAPT, compared to DMSO, as downloaded from NCBI GEO[a]

Gene ID	baseMean	log2FoldChange	lfcSE	stat	pvalue	padj
A1BG	250.2458054	-0.10715732	0.158367876	-0.676635452	0.49863728	0.999958908
A1BG-AS1	40.63079593	0.39664174	0.367504314	1.079284583	0.280460883	0.999958908
AAAS	1731.923126	-0.051556367	0.096066121	-0.536675847	0.591491543	0.999958908
AACS	439.8925232	0.043131776	0.133312758	0.323538244	0.746287649	0.999958908
AADAT	190.0514599	-0.079892132	0.172709659	-0.462580568	0.64366504	0.999958908

[a]The first column represents the GENE ID with symbols according to Human Gene Nomenclature Committee . The second column represents the base mean for all samples which is followed by log2FoldChange and standard error of log2FoldChange (lfcSE). The next column represents the test statistic used to caluclate the pvalue and finally, padj represents the p value adjusted for multiple hypothesis testing using Benjamini-Hochberg method.

The first column corresponds to gene ID or gene name according to HUGO Gene Nomenclature Committee. The second column represents 'the average of the normalized count values, dividing by size factors, taken over all samples' (Love, Anders and Huber, 2014). The other 5 columns are self-explanatory. It is only worth noting that padj column represents the p-value adjusted for the multiple hypothesis testing and the method of doing it applied by default for DESeq2 is Benjamini-Hochberg (Love, Anders and Huber, 2014; Love, Huber and Anders, 2014).

To use the data for GSEAPreranked which is suitable for analysis of RNA sequencing data that contains a list of preranked genes (genes with assigned ranking metric such as log2 fold change, test statistic or p value), I first had to adjust the downloaded data and its file format. The required file format is .rnk or ranked list file format. To do so, I opened .txt file in excel and deleted all columns apart from Gene ID and log2FoldChange. Log2FoldChange was my desired ranking metric. To avoid Java parsing error while loading the file into GSEA, I also deleted the data from the first row (Gene ID and log2FoldChange) but didn't delete the row itself as GSEA ignores the first row during analysis and so deleting the entire row instead of its contents would exclude the first gene from analysis. After saving the file, I just renamed .txt extension to .rnk which is possible without corrupting or damaging the file as both file formats are text based formats. Again, to avoid the parsing error, I renamed the file and folder in which the file was stored to change hyphens to underscores and removed the spaces as only letters, numbers and underscores are allowed. I then loaded the files into GSEA user interface by clicking on *Load data* and choosing the respective .rnk file. Afterwards, I ran GSEAPreranked by clicking on *Run GSEAPreranked* and chose the following settings:

Required fields:

Gene Sets Database- h.all.v2023.1.Hs.symbols.gmt (Hallmark gene sets database from Molecular Signatures Database which 'are coherently expressed signatures derived by aggregating many MSigDB gene sets to represent well-defined biological states or processes.' (https://www.gsea-msigdb.org/gsea/msigdb/)

Number of permutations- 50,000 (Note that the more permutations there are, the more accurate p-values and results. However, the maximum number of permutations possible to be executed within the reasonable amount of time is determined by hardware configuration. The following was run on a laptop with AMD Ryzen 7 5825U Processor with 8 cores, 64GB RAM and 2TB SSD.)

Ranked list- [file_name].rnk

Collapse/Remap to gene symbols- No_collapse (use data set 'as is' in the original format)

Chip platform- BLANK

Basic fields:

Analysis name- [I named the analysis accordingly]

Enrichment statistic- weighted

Max size: exclude larger sets- 500

Min size: exclude smaller sets- 15

Save results in this folder- [I chose the folder accordingly]

Advanced fields (I used the default settings):

Collapsing mode to probe sets-1 gene- Abs_max_of_probes

Normalization mode- meandiv

Seed for permutation- timestamp

Alternate delimiter- BLANK

Create SVG plot images- false

Omit features with no symbol match- true

Make detailed gene set report- true

Plot graphs for the top sets of each phenotype- 20

Make a zipped file with all reports- false

To run the leading edge analysis, I clicked on *Leading edge analysis* button under *Steps in GSEA analysis* group of options in the upper left corner of GSEA user interface. I loaded the GSEA results into the program by selecting the folder with results from previous GSEA analysis and clicking on *Load GSEA results* which loads all gene sets from the analysis together with their calculated parameters. Afterwards, I selected the gene sets that have familywise error rate (FWER) p-value less than 0.05 for both genes with positive NES at the top of the list and genes with negative NES at the bottom of the list and clicked on *Run leading edge analysis* to obtain the results. As the previous analysis is extremely conservative, I repeated the analysis using all gene sets that have a nominal p value less than 0.05 and false discovery rate (FDR) q value less than 0.1. Out of numerous core enrichment genes from each statistically significantly enriched gene set, I chose the ones with the absolute value of rank metric score (= log2FoldChange) greater than 0.58 which corresponds to 50% or more change in the expression value among different treatment conditions.

In order to get the enrichment map of my GSEA results, I first opened the Cytoscape program with installed *EnrichmmentMap* plug-in. I then went back to GSEA user interface and clicked on *Enrichment Map Visualisation* button under *Steps in GSEA analysis* group of options in the upper left corner of GSEA user interface. I loaded the GSEA results in the same manner as described above for leading edge analysis and used the following settings before clicking on *Build Enrichment Map*:

P-value cutoff- 0.05

FDR q-value cut-off- 0.1

Similarity cut-off under advanced options- Jaccard + Overlap combined- 0.375 and
combined constant- 0.5.

Once built, the enrichment map is automatically visible in Cytoscape program and can be manipulated further to obtain publication-like figure. For more details on how to prepare the publication-ready figure, reader is referred to *Nature Protocols* paper giving a very detailed explanation of required steps (Reimand *et al.*, 2019).

4.7. Statistical analysis

4.7.1. Luciferase assays

I performed the statistical analysis and plotted the data in GraphPad Prism software version 9. Prior to inputting the data into the GraphPad, I calculated relative luciferase luminescence values in Microsoft Excel program.

For a single reporter firefly luciferase assay, I first 'subtracted' (not in a mathematical sense as the procedure is actually division) the background basal level of luciferase luminescence in empty vector transfected cells (luciferase reporter only) from cells transfected both with luciferase reporter construct and construct coding for the expression of a protein of interest. To do so, I first took the mean of absolute luminescence (measured by luminometer in relative light units (RLU)) of two wells with untreated, empty vector transfected cells and then divided the absolute luminescence value of each well transfected with both constructs by this mean. In this way, I obtained the relative luciferase luminescence normalized to the background level of luminescence. I entered this data into GraphPad and used it for subsequent analysis.

As for dual luciferase assay system, I had two absolute luminescence values measured per well. One of them is for Firefly luciferase and another one for Renilla. I divided the Firefly luciferase absolute luminescence value by Renilla luciferase absolute luminescence value, separately for each well. This gave me the relative Firefly to Renilla value normalized to internal Renillla control that accounts for different cell number and variable transfection efficiency.

In GraphPad, prior to conducting the statistical significance testing to identify the difference in relative luciferase activity between treatment conditions, I carried out tests for outliers, normality and homoscedasticity (equality of variances). This is necessary to be able to choose the correct significance test- parametric vs non-parametric or parametric with required corrections (Field, 2017).

To identify outliers, I used Robust regression and OUTlier removal (ROUT) method with Q=5% aggressiveness level (Q is the maximum false discovery rate which is to an extent similar to significance level α). I excluded the identified outliers from further analysis.

Following the identification of outliers, I carried out normality testing with Shapiro-Wilk normality test which is especially recommended in case of small sample sizes (N < 10 and down to N = 3). I used the significance level α=0.05. If at least one of the groups of samples was not normally distributed, I performed the non-parametric equivalent of ANOVA test, that is to say Kruskal-Wallis test followed by Dunn's multiple comparisons *post-hoc* test which accounts for family-wise error rate.

If all sample groups were normally distributed, I checked for equality of variances using both Brown-Forsythe and Bartlett's test. If at least one of them was significant meaning heteroscedasticity was present, I performed the Welch ANOVA test. I chose Welch instead of ANOVA with Brown-Forsythe correction because the Welch test has more power while controlling equally well for Type-I error rate (Field, 2017). I followed up Welch ANOVA with Dunnett's T3 multiple comparisons *post-hoc* test. Finally, if all sample groups showed equal variances, I carried out the ordinary one-way ANOVA test followed by Tukey's multiple comparisons test.

Summary of statistical data analysis is given in the Figure 3. below.
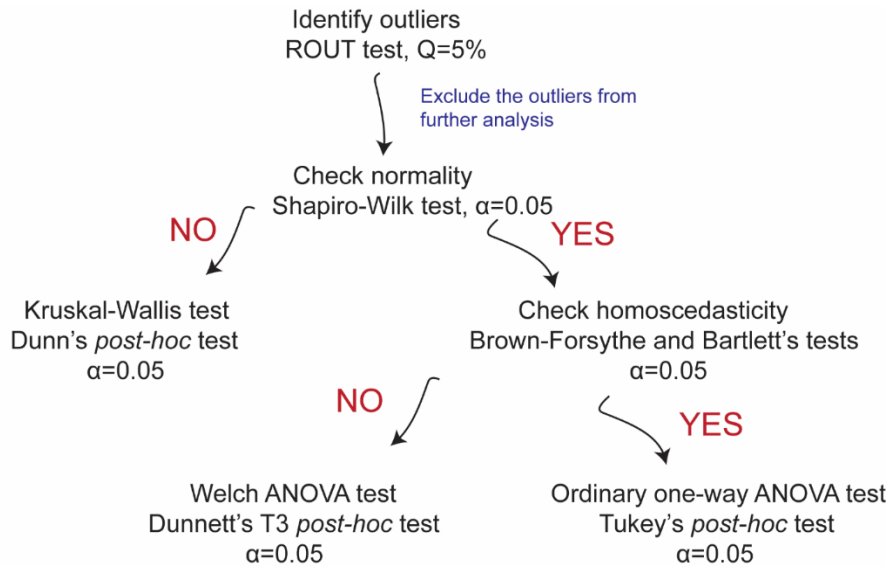
Figure 3. The summary of statistical data analysis. First, the data were checked for outliers using Robust regression and OUTlier removal (ROUT) test with Q=5% aggressiveness level (to an extent similar to significance level α). The outliers were then excluded from further analysis. The next step was to check for normal distribution of the data using Shapiro-Wilk test with α=0.05 significance level. This was the significance level used for all the other tests as well. If the data were not normally distributed, Kruskal-Wallis test was performed with Dunn's post-hoc comparisons. If the data were normally distributed, homoscedasticity was checked using both Brown-Forsythe and Bartlett's tests. If at least one test was significant (no equal variances assumed), Welch's ANOVA test was carried out with Dunnett's T3 post-hoc comparisons. If the data were on the other hand homoscedastic, ordinary one-way ANOVA was performed with Tukey's post-hoc comparisons.

5. Results

5.1. Luciferase assays

5.1.1. HeLa RBPJ KO#42 + NICD-EHEB + RBPJ wt

HeLa RBPJ KO#42 cells were transfected with 250 ng pGa981-6 Firefly luciferase reporter construct that contains 12 EBNA-2 responsive elements which can be bound by RBPJ. Furthermore, the cells were transfected with 10 ng NICD-EHEB (**N**otch-1 **I**ntra**c**ellular **D**omain from human) and 50 ng RBPJ wt constructs. To equalize transfection stress, the appropriate amount of pcDNA3 was used where necessary, which is the vector backbone for all the other plasmids. Cells were then treated with respective amounts of inhibitors as described in the methods section of this thesis and additionally depicted in Figure 4.

Welch's ANOVA test showed a significant effect of different RIN1 inhibitor concentrations on relative luciferase activity with test statistic $W(3.000, 8.768) = 19.65$, $p < 0.001$. Dunnett's T3 *post-hoc* comparisons revealed a significant decrease in relative luciferase activity for RIN1 10 µM concentration compared to DMSO, RIN1 2.5 µM and RIN1 5 µM, with $p < 0.05$ for all three comparisons. Respective mean values and 95% confidence intervals are 544.6 [337.7, 751.4] for DMSO; 640.4 [352.6, 928.2] for RIN1 2.5 µM; 369.4 [222.0, 516.8] for RIN1 5 µM; and 107.1 [74.66, 139.4] for RIN1 10 µM.

Welch's ANOVA test showed a significant effect of different CB-103 inhibitor concentrations on relative luciferase activity with test statistic $W(3.000, 10.570) = 15.25$, $p < 0.001$. Dunnett's T3 *post-hoc* comparisons revealed a significant decrease in relative luciferase activity for CB-103 20 µM and CB-103 40 µM, compared to DMSO control with $p < 0.05$ for both comparisons. Moreover, there was a significant reduction in relative luciferase activity for CB-103 40 µM compared to 10 µM, with $p < 0.01$. Corresponding mean values and 95% confidence intervals are 544.6 [337.7, 751.4] for DMSO; 248.7 [203.8, 293.5] for CB-103 10 µM; 187.7 [116.1, 259.3] for CB-103 for 20 µM; and 112.5 [68.95, 156.1] for CB-103 40 µM.
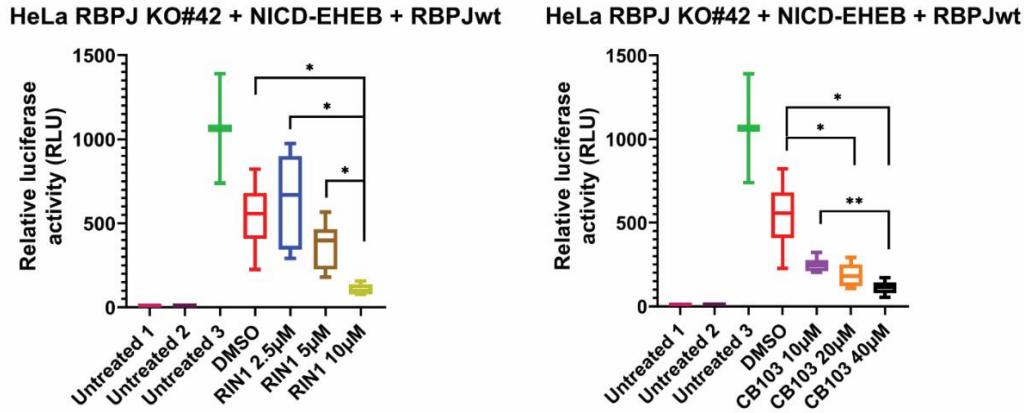
Figure 4. Luciferase assay results for HeLa RBPJ KO#42 + NICD-EHEB + RBPJ wt. HeLa RBPJ KO#42 cells were transfected with 250 ng pGa981-6 Firefly luciferase reporter construct (containing 12 EBNA-2 responsive elements that can be bound by RBPJ), 10 ng NICD-EHEB and 50 ng RBPJ wild type constructs. The cells were then treated with respective amounts of inhibitors as shown on the x-axis of plots. Untreated 1= cells transfected with the reporter construct only, Untreated 2= reporter construct and NICD-EHEB transfected cells, and Untreated 3= untreated cells transfected with reporter construct, NICD-EHEB and RBPJ wt. N=6 wells per inhibitor concentration (including DMSO) and N=2 wells for the Untreated 1, 2, and 3. RLU= relative light units. P-value naming convention: * $p<0.05$, ** $p<0.01$, *** $p<0.001$ and **** $p<0.0001$. Shown is the box-and-whisker plot. The three horizontal lines of box represent 25th percentile (1st quartile), median and 75th percentile (3rd quartile). Whiskers extending from the box represent minimum and maximum values.

5.1.2. HeLa RBPJ KO#42+ RBPJ-VP16

HeLa RBPJ KO#42 cells were transfected with 250 ng pGa981-6 Firefly luciferase reporter construct, 10 ng RBPJ-VP16 construct and appropriate amounts of pcDNA3, where necessary. RBPJ-VP16 is an RBPJ protein fused to herpes simplex virus transcription factor VP16 protein that acts as a strong transactivator. The cells were afterwards treated with respective amounts of inhibitors as depicted in Figure 5.

Ordinary one-way ANOVA test showed a significant effect of different RIN1 inhibitor concentrations on relative luciferase activity with test statistic $F_{(3,20)}= 23.21$, $p<0.0001$. Tukey's *post-hoc* comparisons revealed a significant decrease in relative luciferase activity for RIN1 2.5 µM, 5 µM and 10 µM, compared to DMSO with $p<0.0001$ for all three comparisons. Respective mean values and 95% confidence intervals are 1323.0 [930.3, 1716.0] for DMSO; 528.7 [373.5, 683.9] for RIN1 2.5 µM, 416.1 [253.1, 579.0] for RIN1 5 µM and 276.9 [62.61, 491.3] for RIN1 10 µM.

Ordinary one-way ANOVA test showed a significant effect of different CB-103 inhibitor concentrations on relative luciferase activity with test statistic $F_{(3, 20)}= 9.814$, $p<0.001$. Tukey's *post-hoc* comparisons

revealed a significant decrease in relative luciferase activity for CB-103 10 µM, 20 µM and 40 µM, compared to DMSO with $p<0.01$ for CB-103 10 and 20 µM, and $p<0.001$ for 40 µM. Corresponding mean values and 95% confidence intervals are 1323.0 [930.3, 1716.0] for DMSO; 545.2 [277.5, 812.9] for CB-103 10 µM; 528.6 [117.0, 940.2] for CB-103 20 µM; and 331.4 [-17.67, 680.5] for CB-103 40 µM.

Figure 5. Luciferase assay results for HeLa RBPJ KO#42+ RBPJ-VP16. HeLa RBPJ KO#42 cells were transfected with 250 ng pGa981-6 Firefly luciferase reporter construct (containing RBPJ responsive element), 10 ng RBPJ-VP16 construct and appropriate amounts of pcDNA3, where necessary. N= 6 wells per RIN1 and CB-103 concentration, and for DMSO. N=4 wells for the untreated cells. P-value naming convention: * $p<0.05$, ** $p<0.01$, *** $p<0.001$ and **** $p<0.0001$. Shown is the box-and-whisker plot. The three horizontal lines of box represent 25th percentile (1st quartile), median and 75th percentile (3rd quartile). Whiskers extending from the box represent minimum and maximum values.
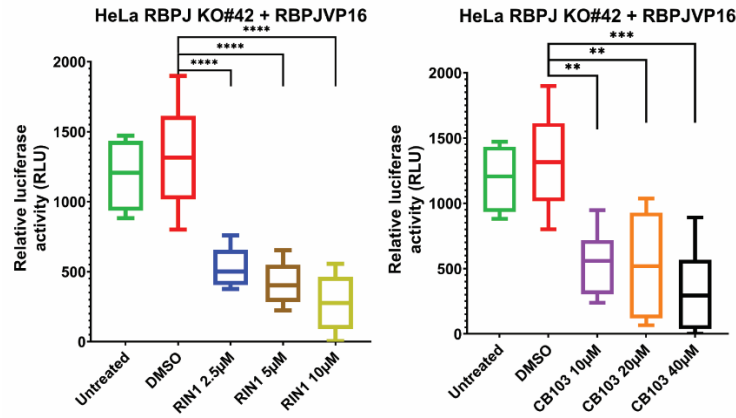
5.1.3. HeLa RBPJ KO#42+ RBPJ-VP16-DM(F261A/L388A)

HeLa RBPJ KO#42 cells were transfected with 250 ng pGa981-6 Firefly luciferase reporter construct, 10 ng RBPJ-VP16-DM(F261A/L388A) construct and appropriate amounts of pcDNA3, where necessary. RBPJ-VP16-DM(F261A/L388A) is an RBPJ-VP16 fusion protein with two mutations in RBPJ rendering it almost deficient for Notch-cofactor binding. The cells were afterwards treated with respective amounts of inhibitors as depicted in Figure 6.

Ordinary one-way ANOVA test showed a significant effect of different RIN1 inhibitor concentrations on relative luciferase activity with test statistic $F_{(3,20)}= 21.82$, $p<0.0001$. Tukey's *post-hoc* comparisons revealed a significant decrease in relative luciferase activity for RIN1 2.5 µM, 5 µM and 10 µM, compared to DMSO with $p<0.001$ for RIN1 2.5 µM, and $p<0.0001$ for 5 µM and 10 µM. Respective mean values and

95% confidence intervals are 1512 [1152.0, 1871.0] for DMSO; 615.8 [500.2, 731.4] for RIN1 2.5 µM; 527.8 [183.5, 872.2] for RIN1 5 µM; and 285.1 [-10.37, 580.6] for RIN1 10 µM.

Welch's ANOVA test showed a significant effect of different CB-103 inhibitor concentrations on relative luciferase activity with test statistic W(3.000,10.53)= 20.20, p=0.0001. Dunnett's T3 $post$-hoc comparisons revealed a significant decrease in relative luciferase activity for CB-103 10 µM, 20 µM and 40 µM, compared to DMSO with p<0.01 in all three cases. Additionally, there was a significant decrease in relative luciferase activity for CB-103 40 µM compared to 10 µM with p<0.01, and 20 µM with p<0.05. Corresponding mean values and 95% confidence intervals are 1512 [1152.0, 1871.0] for DMSO; 633.5 [518.4, 748.6] for CB-103 10 µM; 537.8 [459.4, 616.2] for CB-103 20 µM; and 354.1 [233.3, 474.9] for CB-103 40 µM.

Figure 6. Luciferase assay results for HeLa RBPJ KO#42+ RBPJ-VP16-DM(F261A/L388A). HeLa RBPJ KO#42 cells were transfected with 250 ng pGa981-6 Firefly luciferase reporter construct, 10 ng RBPJ-VP16-DM construct (harboring two RBPJ mutations severely impairing the Notch-cofactor binding) and appropriate amounts of pcDNA3, where necessary. N= 6 wells per RIN1 and CB-103 concentration, and for DMSO. N=4 wells for the untreated cells. P-value naming convention: * p<0.05, ** p<0.01, *** p<0.001 and **** p<0.0001. Shown is the box-and-whisker plot. The three horizontal lines of box represent 25th percentile (1st quartile), median and 75th percentile (3rd quartile). Whiskers extending from the box represent minimum and maximum values.

5.1.4. HeLa RBPJ KO#42+ RBPJ-VP16-NBM

HeLa RBPJ KO#42 cells were transfected with 250 ng pGa981-6 Firefly luciferase reporter construct, 10 ng RBPJ-VP16-NBM (E398R/F261A/V263A/R422E/E425R) construct and appropriate amounts of pcDNA3, where necessary. RBPJ-VP16-NBM is an RBPJ-VP16 fusion protein with five mutations in RBPJ rendering

it deficient for Notch-cofactor binding. The cells were afterwards treated with respective amounts of inhibitors as depicted in Figure 7.

Ordinary one-way ANOVA test showed a significant effect of different RIN1 concentrations on relative luciferase activity with test statistic $F_{(3,20)}=7.116$, $p<0.01$. Tukey's *post-hoc* comparisons revealed a significant decrease in relative luciferase activity for RIN1 2.5 µM, 5 µM and 10 µM compared to DMSO, with $p<0.05$ for RIN1 2.5 µM, and $p<0.01$ for 5 µM and 10 µM. Respective mean values and 95% confidence intervals are 631 [390.7, 871.3] for DMSO; 272.6 [86.18, 459.0] for RIN1 2.5 µM; 228.4 [56.14, 400.6] for RIN1 5 µM; and 181.2 [-3.962, 366.5] for RIN1 10 µM.

Welch's ANOVA test showed a significant effect of different CB-103 concentrations on relative luciferase activity with test statistic $W_{(3.00,10.58)}= 8.812$, $p<0.01$. Dunnett's T3 *post-hoc* comparisons revealed a significant decrease in relative luciferase activity for CB-103 10 µM, 20 µM and 40 µM, compared to DMSO, with $p<0.05$ in all three cases. Corresponding mean values and 95% confidence intervals are 631 [390.7, 871.3] for DMSO; 260.4 [180.1, 340.6] for CB-103 10 µM; 178.6 [119.3, 237.9] for CB-103 20 µM; and 127.5 [34.04, 221.0] for CB-103 40 µM.

Figure 7. Luciferase assay results for HeLa RBPJ KO#42+ RBPJ-VP16-NBM. HeLa RBPJ KO#42 cells were transfected with 250 ng pGa981-6 Firefly luciferase reporter construct, 10 ng RBPJ-VP16-NBM construct (harboring five RBPJ mutations severely impairing the Notch-cofactor binding) and appropriate amounts of pcDNA3, where necessary. N= 6 wells per RIN1 and CB-103 concentration, and for DMSO. N=3 wells for the untreated cells. P-value naming convention: * p<0.05, ** p<0.01, *** p<0.001 and **** p<0.0001. Shown is the box-and-whisker plot. The three horizontal lines of box represent 25th percentile (1st quartile), median and 75th percentile (3rd quartile). Whiskers extending from the box represent minimum and maximum values.
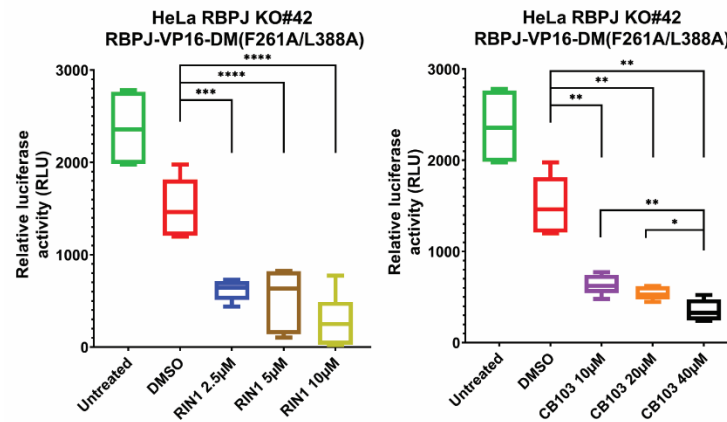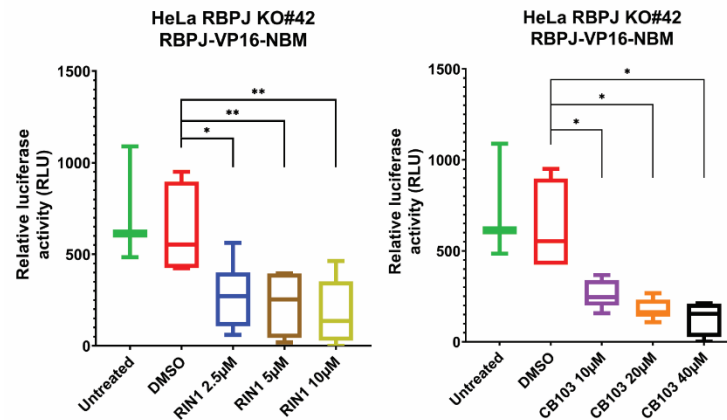
5.1.5. HeLa RBPJ KO#42+ Gal4-VP16-1

HeLa RBPJ KO#42 cells were transfected with 250 ng pFr-luc Firefly luciferase reporter construct, 10 ng Gal4-VP16-1 and appropriate amounts of pcDNA3, where necessary. pFr-luc is the reporter construct having a DNA binding element for Gal4 DNA-binding protein. Gal4-VP-16-1 is the fusion protein consisting of Gal4 DNA binding domain which binds to upstream activating sequence (UAS), and VP16 transactivation domain. The cells were afterwards treated with respective amounts of inhibitors as depicted in Figure 8.

Ordinary one-way ANOVA test showed a significant effect of different RIN1 concentrations on relative luciferase activity with test statistic $F_{(3,20)}=36.70$, $p<0.0001$. Tukey's *post-hoc* comparisons revealed a significant decrease in relative luciferase activity for RIN1 2.5 µM, 5 µM and 10 µM, compared to DMSO with $p<0.0001$ for all three comparisons. Respective mean values and 95% confidence intervals are 1511 [1108, 1915] for DMSO; 301.5 [149.4, 453.6] for RIN1 2.5 µM, 318.2 [98.93, 537.5] for RIN1 5 µM; and 245.8 [56.28, 435.2] for RIN1 10 µM.

Welch's ANOVA test showed a significant effect of different CB-103 concentrations on relative luciferase activity with test statistic $W_{(3.00,9.262)}= 17.05$, $p<0.001$. Dunnett's T3 *post-hoc* comparisons revealed a significant decrease in relative luciferase activity for CB-103 10 µM, 20 µM and 40 µM, compared to DMSO, with $p<0.05$ for 10 µM, $p<0.01$ for 20 µM and $p<0.001$ for 40 µM. Moreover, there was a significant decrease in relative luciferase activity for CB-103 40 µM compared to 10 µM with $p<0.05$. Corresponding mean values and 95% confidence intervals are 1511 [1108, 1915] for DMSO; 707.3 [460.2, 954.4] for CB-103 10 µM; 465.1 [400.4, 529.8] for CB-103 20 µM; and 249.5 [56.44, 442.6] for CB-103 40 µM.
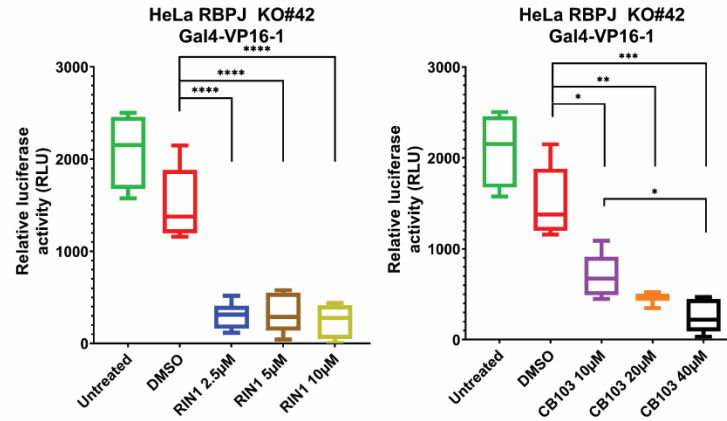
Figure 8. Luciferase assay results for HeLa RBPJ KO#42+ Gal4-VP16-1. HeLa RBPJ KO#42 cells were transfected with 250 ng pFr-luc Firefly luciferase reporter construct (containing the Gal4 responsive element), 10 ng Gal4-VP16-1 construct and appropriate amounts of pcDNA3, where necessary. N= 6 wells per RIN1 and CB-103 concentration, and for DMSO. N=4 wells for the untreated cells. P-value naming convention: * $p<0.05$, ** $p<0.01$, *** $p<0.001$ and **** $p<0.0001$. Shown is the box-and-whisker plot. The three horizontal lines of box represent 25th percentile (1st quartile), median and 75th percentile (3rd quartile). Whiskers extending from the box represent minimum and maximum values.

5.1.6. HeLa RBPJ KO#42+ Firefly(Gal4-VP16)+ Renilla(TK)

HeLa RBPJ KO#42 cells were transfected with 250 ng pFr-luc Firefly luciferase reporter construct, 10 ng Gal4-VP16-1 and 25 ng pRL-TK, as well as appropriate amounts of pcDNA3, where necessary. pRL-TK is the Renilla luciferase enzyme with low constitutive expression under the herpes simplex virus thymidine kinase promoter. The cells were afterwards treated with respective amounts of inhibitors as depicted in Figure 9. Figure 10. shows the absolute Renilla luciferase activity in RLU, for different RIN1 and CB-103 concentrations, respectively.

Kruskal-Wallis test showed a significant effect of different RIN1 concentrations on relative Firefly to Renilla luciferase activity with test statistic H(3)= 14.17, $p<0.01$. Dunn's *post-hoc* comparisons revealed a significant decrease in relative luciferase activity for RIN1 5 µM and 10 µM concentrations, compared to DMSO, with $p<0.05$ for RIN1 5 µM, and $p<0.01$ for 10 µM. Respective median values and 95% confidence intervals are 9.407 [9.011, 14.16] for DMSO; 1.701 [0.7982, 3.353] for RIN1 2.5 µM; 1.297 [0.5837, 2.852] for RIN1 5 µM; and 0.8744 [0.4891, 2.609] for RIN1 10 µM.

Ordinary one-way ANOVA test did not show a significant effect of different RIN1 concentrations on absolute Renilla luciferase activity with test statistic F(3,20)= 2.708, $p>0.05$. Tukey's *post-hoc* comparisons confirmed no significant difference between any of the concentration groups. Respective mean values and

95% confidence intervals are 81755 [48613, 114897] for DMSO; 99595 [66463, 132727] for RIN1 2.5 µM; 132928 [102500, 163357] for RIN1 5 µM; and 79968 [27353, 132583] for RIN1 10 µM.

Kruskal-Wallis test showed a significant effect of different CB-103 concentrations on relative Firefly to Renilla luciferase activity with test statistic H(3)= 16.65, $p<0.001$. Dunn's *post-hoc* comparisons revealed a significant decrease in relative luciferase activity for CB-103 20 µM and 40 µM, compared to DMSO, with $p<0.05$ for CB-103 20 µM, and $p<0.001$ for 40 µM. Corresponding median values and 95% confidence intervals are 9.407 [9.011, 14.16] for DMSO; 5.324 [2.888, 6.498] for CB-103 10 µM; 3.337 [2.400, 4.459] for CB-103 20 µM; and 2.515 [1.861, 4.161] for CB-103 40 µM.

Ordinary one-way ANOVA test did not show a significant effect of different CB-103 concentrations on absolute Renilla luciferase activity with test statistic F(3,20)= 2.242, $p>0.05$. Tukey's *post-hoc* comparisons confirmed no significant difference between any of the concentration groups. Corresponding mean values and 95% confidence intervals are 81755 [48613, 114897] for DMSO; 59353 [24931, 93776] for CB-103 10 µM; 58465 [38727, 78203] for CB-103 20 µM; and 43525 [27573, 59477] for CB-103 40 µM.
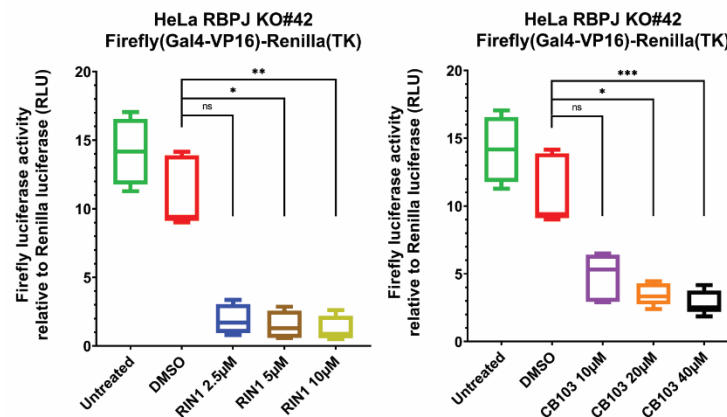
Figure 9. Luciferase assay results for HeLa RBPJ KO#42+ Firefly(Gal4-VP16)+ Renilla(TK). HeLa RBPJ KO#42 cells were transfected with 250 ng pFr-luc Firefly luciferase reporter construct, 10 ng Gal4-VP16-1 and 25 ng pRL-TK construct (Renilla luciferase gene under the constitutively expressed thymidine kinase promoter from the herpes simplex virus). N= 6 wells per RIN1 and CB-103 concentration, and for DMSO. N=4 wells for the untreated cells. P-value naming convention: * p<0.05, ** p<0.01, *** p<0.001 and **** p<0.0001. Shown is the box-and-whisker plot. The three horizontal lines of box represent 25th percentile (1st quartile), median and 75th percentile (3rd quartile). Whiskers extending from the box represent minimum and maximum values.

Figure 10. Luciferase assay results of absolute Renilla luciferase activity for HeLa RBPJ KO#42+ Firefly(Gal4-VP16)+ Renilla(TK). RBPJ KO#42 cells were transfected with 250 ng pFr-luc Firefly luciferase reporter construct, 10 ng Gal4-VP16-1 and 25 ng pRL-TK construct (Renilla luciferase gene under the constitutively expressed thymidine kinase promoter from the herpes simplex virus). N= 6 wells per RIN1 and CB-103 concentration, and for DMSO. N=4 wells for the untreated cells. P-value naming convention: * $p<0.05$, ** $p<0.01$, *** $p<0.001$ and **** $p<0.0001$. Shown is the box-and-whisker plot. The three horizontal lines of box represent 25th percentile (1st quartile), median and 75th percentile (3rd quartile). Whiskers extending from the box represent minimum and maximum values.

5.1.7.   HeLa RBPJ KO#42+ SV40-luciferase

HeLa RBPJ KO#42 cells were transfected with either 250 ng of pGl3 basic or 250 ng of pGl3 control plasmid. pGl3 basic is an empty vector construct with Firefly luciferase gene under no promoter. pGl3 control is the construct containing the Firefly luciferase gene under the strong constitutively active Simian virus 40 promoter. The cells were afterwards treated with respective amounts of inhibitors as depicted in Figure 11.

Ordinary one-way ANOVA showed a significant effect of different RIN1 concentrations on relative luciferase activity with test statistic $F(3,36)= 5.217$, $p<0.01$. Tukey's *post-hoc* comparisons revealed a significant decrease in relative luciferase activity only for the highest RIN1 10 µM concentration, compared to DMSO, with $p<0.05$. What is more, the relative luciferase activity is significantly lower for RIN1 10 µM, compared to RIN1 2.5 µM and 5 µM, with $p<0.01$, and $p<0.05$, respectively. Respective mean values and 95% confidence intervals are 1144 [950.9, 1337] for DMSO; 1272 [1027, 1517] for RIN1 2.5 µM; 1184 [994.1, 1375] for RIN1 5 µM; and 764.8 [513.2, 1016] for RIN1 10 µM.

Welch's ANOVA test showed a significant effect of different CB-103 concentrations on relative luciferase activity with test statistic $W(3.000, 10.73)= 15.97$, $p<0.001$. Dunnett's T3 *post-hoc* comparisons revealed a

significant decrease in relative luciferase activity for CB-103 10 µM, 20 µM and 40 µM, compared to DMSO, with $p<0.05$ for CB-103 10 µM, and $p<0.01$ for 20 µM and 40 µM. Moreover, the relative luciferase activity for CB-103 40 µM was significantly lower than that of 10 µM with $p<0.01$. Corresponding mean values and 95% confidence intervals are 1299 [875.6, 1721] for DMSO; 515.4 [406.9, 624.0] for CB-103 10 µM; 349.7 [212.7, 486.7] for CB-103 20 µM; and 232.1 [123.6, 340.6] for CB-103 40 µM.
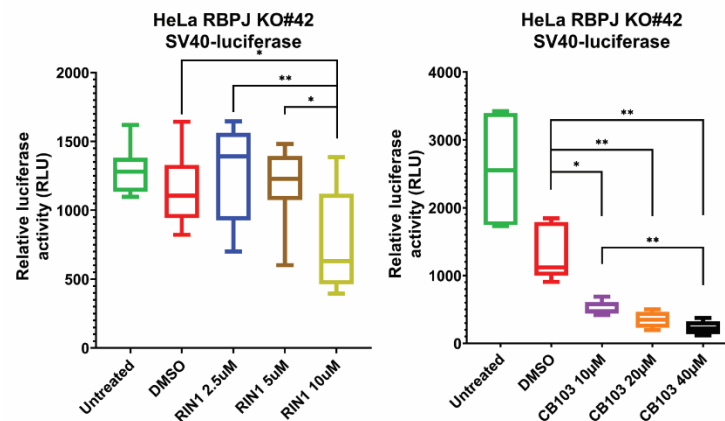
Figure 11. Luciferase assay results for HeLa RBPJ KO#42+ SV40-luciferase. HeLa RBPJ KO#42 cells were transfected with either 250 ng of pGl3 basic (empty vector) or 250 ng of pGl3 control constructs (Firefly luciferase gene under the strong constitutively active Simian virus 40 promoter). N= 10 wells per RIN1concentration, and for DMSO in a separate 'RIN1 experiment'. N=6 wells for the untreated cells in the separate 'RIN1 experiment'. N=6 wells per CB-103 concentration, and for DMSO in the separate 'CB-103 experiment'. N= 4 wells for the untreated cells in the separate 'CB-103 experiment'. P-value naming convention: * p<0.05, ** p<0.01, *** p<0.001 and **** p<0.0001. Shown is the box-and-whisker plot. The three horizontal lines of box represent 25th percentile (1st quartile), median and 75th percentile (3rd quartile). Whiskers extending from the box represent minimum and maximum values.

5.1.8. HeLa RBPJ KO#42+ Gal4-p65 (RelA)

HeLa RBPJ KO#42 cells were transfected with 250 ng pFr-luc Firefly luciferase reporter construct, 10 ng Gal4-p65 (RelA) and appropriate amounts of pcDNA3, where necessary. Gal4-p65 is the fusion protein containing Gal4 which is a DNA-binding domain which binds to Gal4 responsive element (also known as Upstream Activation Sequence (UAS)) and p65 transactivation domain also known as RelA. RelA is one of the two subunits forming NF-kappa B, together with p50. The cells were afterwards treated with respective amounts of RIN1 inhibitor as depicted in Figure 12.

Kruskal-Wallis test showed a significant effect of different RIN1 concentrations on relative luciferase activity with test statistic H(3)= 32.29, $p<0.0001$. Dunn's *post-hoc* comparisons revealed a significant decrease of relative luciferase activity for RIN1 5 µM and 10 µM, compared to DMSO, with $p<0.01$ for RIN1 5 µM, and $p<0.0001$ for 10 µM. Furthermore, the relative luciferase activity was significantly lower for RIN1 10 µM compared to 2.5 µM with $p<0.01$. Respective median values and 95% confidence intervals are 1644 [1534, 3027] for DMSO; 799.4 [404.5, 984.7] for RIN1 2.5 µM; 542.7 [247.0, 620.5] for RIN1 5 µM; and 198.2 [117.2, 307.5] for RIN1 10 µM.
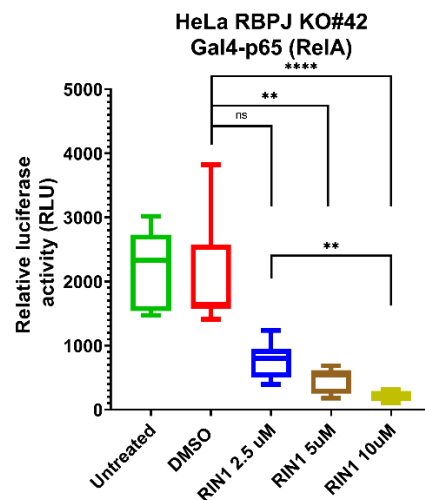
Figure 12. Luciferase assay results for HeLa RBPJ KO#42+ Gal4-p65 (RelA). HeLa RBPJ KO#42 cells were transfected with 250 ng pFr-luc Firefly luciferase reporter construct, 10 ng Gal4-p65 (RelA) and appropriate amounts of pcDNA3, where necessary. N= 10 wells per RIN1 concentration, and for DMSO. N=6 wells for the untreated cells. P-value naming convention: * p<0.05, ** p<0.01, *** p<0.001 and **** p<0.0001. Shown is the box-and-whisker plot. The three horizontal lines of box represent 25th percentile (1st quartile), median and 75th percentile (3rd quartile). Whiskers extending from the box represent minimum and maximum values.

5.1.9. HeLa RBPJ KO#42+ RelA(p65) titration

RelA titration experiment was performed in order to determine the optimal RelA plasmid concentration for the next luciferase experiment in which the aim was to investigate the potential inhibitory effects of RIN1 on RelA's transactivation ability.

HeLa RBPJ KO#42 cells were transfected with 250 ng 3xNFκB-luci and 5, 10, 20, 40, 80, 100 and 150 ng RelA construct (Figure 13.). Empty vector backbone pcDNA3 was used to equalize the transfection stress. 3xNFκB-luci is a plasmid encoding for Firefly luciferase gene placed under the control of RelA responsive element.

Ordinary one-way ANOVA test showed a significant effect of different RelA amounts on relative luciferase activity in untreated cells, with test statistic $F_{(6,35)}= 4.996$, $p<0.001$. Tukey's *post-hoc* comparisons revealed a significant increase in relative luciferase activity for all tested amounts of RelA apart from 10 ng, compared to 5 ng RelA. Corresponding p values are $p<0.01$ for 20 ng RelA, $p<0.05$ for 40 ng RelA, $p<0.01$ for 80 ng RelA, $p<0.05$ for 100 ng RelA, and $p<0.01$ for 150 ng RelA, compared to 5 ng RelA. Tukey's *post-hoc* comparisons did not reveal any significant difference in relative luciferase activity for any other possible combinations of RelA amounts, apart from the ones described above. Respective mean values and 95% confidence intervals are 12.33 [7.204, 17.46] for 5 ng RelA; 23.57 [13.28, 33.86] for 10 ng RelA; 32.68 [23.04. 42.32] for 20 ng RelA; 29.21 [16.97, 41.46] for 40 ng RelA; 34.40 [27.08. 41.72] for 80 ng RelA; 30.22 [23.07, 37.38] for 100 ng RelA; and 32.62 [24.32, 40.91] for 150 ng RelA.

Figure 13. Luciferase assay results for HeLa RBPJ KO#42+ RelA(p65) titration. HeLa RBPJ KO#42 cells were transfected with 250 ng 3xNFκB-luci reporter construct (Firefly luciferase gene under the control of RelA responsive element) and 5, 10, 20, 40, 80, 100 and 150 ng RelA construct. Appropriate amounts of empty vector backbone pcDNA3 were used to equalize the transfection stress. N= 6 wells per RelA transfected amount. P-value naming convention: * $p<0.05$, ** $p<0.01$, *** $p<0.001$ and **** $p<0.0001$. Shown is the box-and-whisker plot. The three horizontal lines of box represent 25th percentile (1st quartile), median and 75th percentile (3rd quartile). Whiskers extending from the box represent minimum and maximum values.

5.1.10. HeLa RBPJ KO#42+ 3xNFκB luciferase-RelA(p65)

HeLa RBPJ KO#42 cells were transfected with 250 ng 3xNFκB Firefly luciferase reporter construct, 30 ng RelA and appropriate amounts of pcDNA3, where necessary. The cells were afterwards treated with respective amounts of RIN1 inhibitor as depicted in Figure 14.

Ordinary one-way ANOVA test showed a significant effect of different RIN1 concentrations on relative luciferase activity with test statistic $F(3,36)= 5.066$, $p<0.01$. Tukey's *post-hoc* comparisons revealed a significant decrease in relative luciferase activity for RIN1 10 µM, compared to DMSO, with $p<0.01$. Moreover, the relative luciferase activity was significantly lower for RIN1 10 µM compared to 2.5 µM, with $p<0.05$. Tukey's *post-hoc* comparisons did not reveal a significant change in relative luciferase activity for RIN1 2.5 µM and 5 µM compared to DMSO. Respective mean values and 95% confidence intervals are 29.34 [25.00, 33.68] for DMSO; 28.83 [21.86, 35.80] for RIN1 2.5 µM; 25.18 [21.32, 29.03] for RIN1 5 µM; and 18.81 [15.22, 22.41] for RIN1 10 µM.
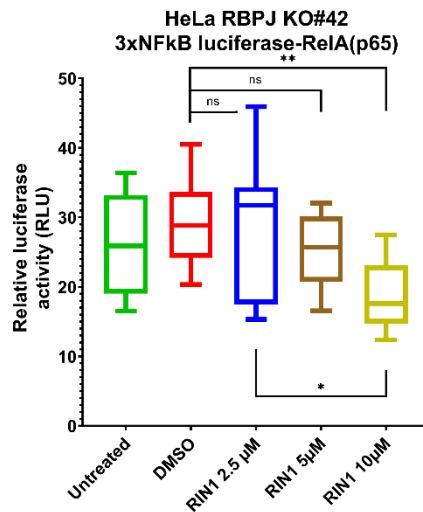
Figure 14. Luciferase assay results for HeLa RBPJ KO#42+ 3xNFκB luciferase-RelA(p65). HeLa RBPJ KO#42 cells were transfected with 250 ng 3xNFκB Firefly luciferase reporter construct, 30 ng RelA construct and appropriate amounts of pcDNA3, where necessary. N= 10 wells per RIN1 concentration, and for DMSO. N=6 wells for the untreated cells. P-value naming convention: * p<0.05, ** p<0.01, *** p<0.001 and **** p<0.0001. Shown is the box-and-whisker plot. The three horizontal lines of box represent 25th percentile (1st quartile), median and 75th percentile (3rd quartile). Whiskers extending from the box represent minimum and maximum values.

5.1.11. HeLa RBPJ KO#42+ HNF6wt-VP16

HeLa RBPJ KO#42 cells were transfected with 250 ng phsHNF6-luc Firefly luciferase reporter construct, 50 ng HNF6wt-VP16 and appropriate amounts of pcDNA3, where necessary. phsHNF6-luc is the luciferase reporter construct with hepatocyte nuclear factor 6 responsive element. HNF6wt-VP16 is the fusion protein consisting of hepatocyte nuclear factor 6 which is both the DNA-binding domain and a transcriptional activator, if used on its own, and VP16 transactivator. The cells were afterwards treated with respective amounts of RIN1 inhibitor as depicted in Figure 15.

Ordinary one-way ANOVA test showed a significant effect of different RIN1 concentrations on relative luciferase activity with test statistic $F(3,36)= 46.33$, $p<0.0001$. Tukey's *post-hoc* comparisons revealed a significant decrease in relative luciferase activity for RIN1 2.5 µM, 5 µM and 10 µM, compared to DMSO with $p<0.0001$ for all three comparisons. What is more, the relative luciferase activity for RIN1 10 µM was significantly lower compared to RIN1 2.5 µM and 5 µM, with $p<0.0001$ and $p<0.01$, respectively. Corresponding mean values and 95% confidence intervals are 181.9 [157.6, 206.2] for DMSO; 118.0 [104.5, 131.5] for RIN1 2.5 µM; 94.85 [76.84, 112.9] for RIN1 5 µM; and 49.22 [33.33, 65.10] for RIN1 10 µM.
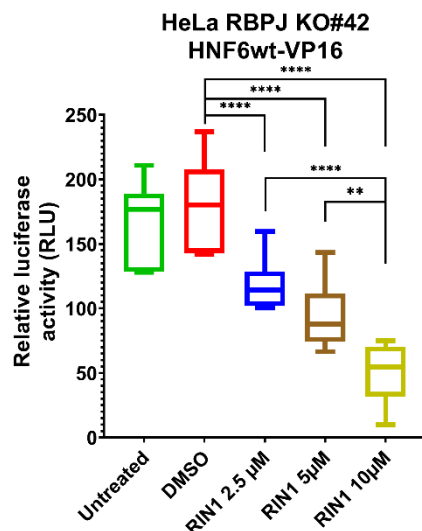
Figure 15. Luciferase assay results for HeLa RBPJ KO#42+ HNF6wt-VP16. HeLa RBPJ KO#42 cells were transfected with 250 ng phsHNF6-luc Firefly luciferase reporter construct (Firefly luciferase gene placed under the hepatocyte nuclear factor 6 responsive element), 50 ng HNF6wt-VP16 and appropriate amounts of pcDNA3, where necessary. N= 10 wells per RIN1 concentration, and for DMSO. N=6 wells for the untreated cells. P-value naming convention: * $p<0.05$, ** $p<0.01$, *** $p<0.001$ and **** $p<0.0001$. Shown is the box-and-whisker plot. The three horizontal lines of box represent 25th percentile (1st quartile), median and 75th percentile (3rd quartile). Whiskers extending from the box represent minimum and maximum values.

5.1.12. HeLa RBPJ KO#42+ Flag1-HNF6wt

HeLa RBPJ KO#42 cells were transfected with 250 ng phsHNF6-luc Firefly luciferase reporter construct, 50 ng Flag1-HNF6wt and appropriate amounts of pcDNA3, where necessary. Flag1-HNF6wt is the Flag1-tagged wild type hepatocyte nuclear factor 6. The cells were afterwards treated with respective amounts of RIN1 inhibitor as depicted in Figure 16.

Kruskal-Wallis test showed a significant effect of different RIN1 concentrations on relative luciferase activity with test statistic H(3)= 26.45, $p<0.0001$. Dunn's *post-hoc* comparisons revealed a significant decrease in relative luciferase activity for RIN1 5 µM and 10 µM, compared to DMSO, with $p<0.05$ and $p<0.0001$, respectively. Furthermore, there was a significant decrease in relative luciferase activity for RIN1 10 µM compared to 2.5 µM with $p<0.01$. Respective median values and 95% confidence intervals are 54.47 [42.59, 69.29] for DMSO; 46.82 [27.18, 67.71] for RIN1 2.5 µM; 34.97 [26.47, 38.12] for RIN1 5 µM; and 17.68 [14.82, 27.82] for RIN1 10 µM.
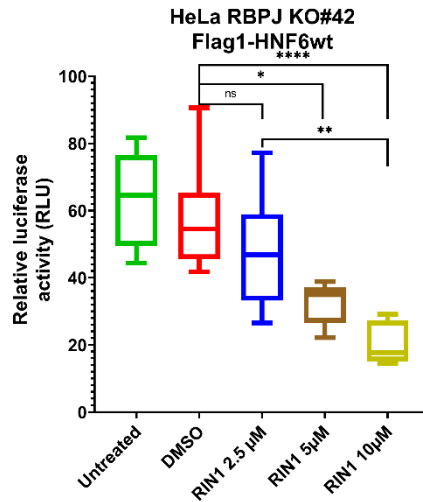
Figure 16. Luciferase assay results for HeLa RBPJ KO#42+ Flag1-HNF6wt. HeLa RBPJ KO#42 cells were transfected with 250 ng phsHNF6-luc Firefly luciferase reporter construct, 50 ng Flag1-HNF6wt and appropriate amounts of pcDNA3, where necessary. N= 10 wells per RIN1 concentration, and for DMSO. N=6 wells for the untreated cells. P-value naming convention: * $p<0.05$, ** $p<0.01$, *** $p<0.001$ and **** $p<0.0001$. Shown is the box-and-whisker plot. The three horizontal lines of box represent 25th percentile (1st quartile), median and 75th percentile (3rd quartile). Whiskers extending from the box represent minimum and maximum values.

5.2. Immunofluorescence assay

HeLa wt cells were seeded onto the slides placed into the compartments of a square Petri dish and treated with respective amounts of inhibitors as shown in Table 1. in the section 4.3.2. The immunofluorescence assay was performed 24 hours after inhibitor treatment whereby the cells were fixed, permeabilized and incubated with the primary antibody against RBPJ-k. Afterwards, the secondary anti-rat Alexa Fluor 488 antibody, which is conjugated to a bright green-fluorescent dye, was added that bound the Fc region of primary antibody. This allowed the visualization of RBPJ-k subcellular localization represented as the green color on the photos taken with fluorescence microscope. Moreover, nuclei were stained with DAPI which fluoresces blue. Additionally, 3 negative controls with untreated HeLa wt and Hela RBPJ KO#42 cell lines were employed. The first HeLa wt control was stained with both primary and secondary antibodies while the second one was stained only with the secondary antibody. The third control consisted of HeLa RBPJ KO#42 cell line stained with both primary and secondary antibodies. The nuclei of all three controls were stained with DAPI.

As shown in Figure 17., the first column, HeLa wt untreated cells stained with both antibodies exhibited the strong green fluorescence primarily concentrated in the oval elongated shape with much weaker and barely visible fluorescence signal in the background in the shape of a cell. HeLa wt untreated cells stained only with the secondary antibody showed almost no distinct green signal apart from some very weak fluorescence in the shape of a cell. The same holds true for HeLa RBPJ KO#42 untreated cells stained with both antibodies. The second column in all three cases shows the clearly visible DAPI-stained blue fluorescent nuclei. The third column represents two merged images, namely that of antibody stained RBPJ-κ (where present) and DAPI-stained nucleus which allows the determination of subcellular localization of RBPJ-κ. In case of HeLa wt untreated cells stained with both antibodies (first row), one can observe that the location of green oval shapes representing the location of RBPJ-κ matches that of blue DAPI-stained nuclei which is further confirmed with cyan-colored nuclei in the merged image. As for HeLa wt untreated cells stained only with secondary antibody and HeLa RBPJ KO#42 untreated cells stained with both antibodies (the second and third row, respectively), one can see the absence of green fluorescence apart from the very weak background signal in the shape of a cell, which when merged with the distinct blue DAPI-stained nuclei gives almost exclusively blue colored nuclei.

The first column in Figure 18. depicts HeLa wt cells treated with either DMSO control or respective amounts of inhibitors and stained with both antibodies while the second column shows the same cells but in a different fluorescence channel which allows for the visualization of blue DAPI stained nuclei. The third column are again merged photos of antibody staining (primary and secondary) and DAPI staining. With regards to DMSO control and all chosen RIN1 and CB-103 inhibitor concentrations, one can observe the same scenario as in case of HeLa wt untreated cells stained with both antibodies. Briefly, there is a strong green fluorescence in the shape of nucleus with minimum background fluorescence in the shape of a cell which corresponds to RBPJ-k staining. This green fluorescence when merged with distinctly DAPI stained blue nuclei, produces the cyan shaped nuclei.
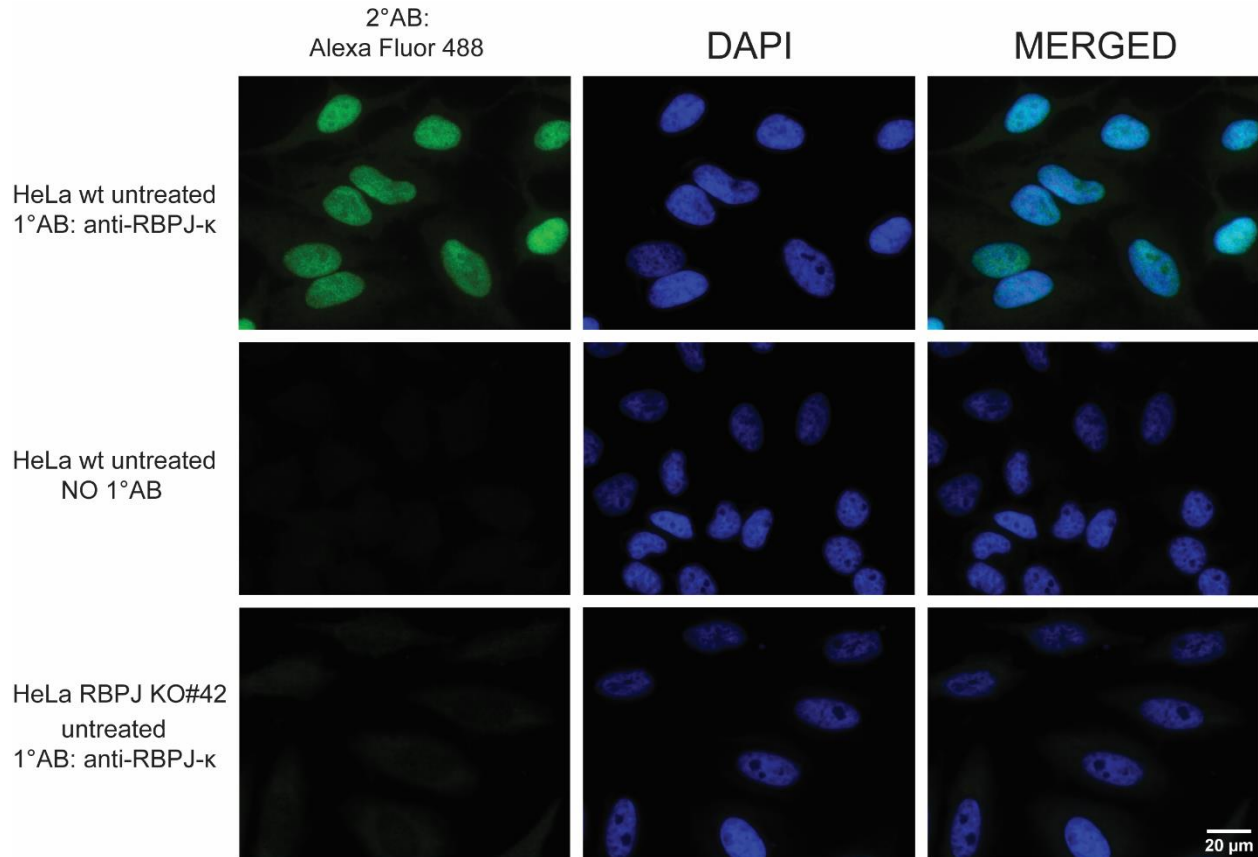
Figure 17. Fluorescence images of HeLa wt and HeLa RBPJ KO#42 untreated cells for checking the subcellular localization of RBPJ. The immunofluorescence assay was performed using anti-RBPJ-κ primary antibody and anti-rat Alexa Fluor 488 secondary antibody. The first column represents either HeLa wt or HeLa RBPJ KO#42 cells either stained or not stained with the primary antibody (as indicated in the figure), that were all stained with the secondary antibody. This either gives or not, the green fluorescence. The second column shows DAPI stained nuclei fluorescing blue while the last column shows merged fluorescence images of the first and second column. All images were taken with 600x magnification. Scale bar is inserted into the last image and pertains to all other images in this figure.
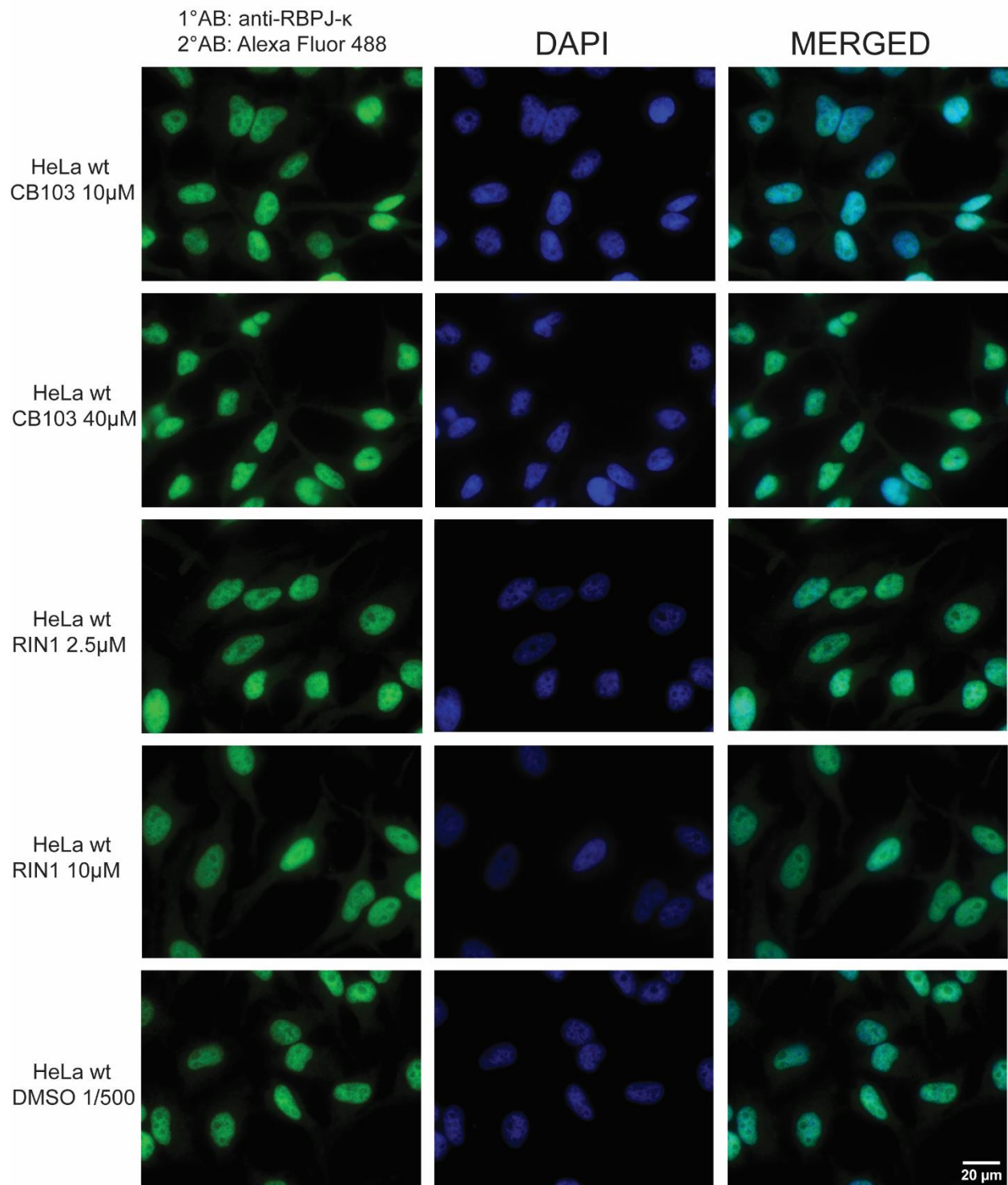
Figure 18. Fluorescence images of HeLa wt cells treated with respective concentrations of RIN1 and CB-103 inhibitors in order to check for the subcellular localization of RBPJ. The immunofluorescence assay was performed using anti-RBPJ-κ primary antibody and anti-rat Alexa Fluor 488 secondary antibody. The first column shows HeLa wt cells treated with respective amounts of inhibitors and stained with both

primary and secondary antibody. This gives the green fluorescence coming from the stained RBPJ-κ. The second column shows DAPI stained nuclei which fluoresce blue and the third column represents merged images from the first and second column. One can observe the colocalization of green and blue fluorescence which, when merged, gives the cyan blue color. All images were taken with 600x magnification. Scale bar is inserted into the last image and pertains to all other images in this figure.

5.3. Gene Set Enrichment Analysis (GSEA), Leading edge-analysis (LEA) and enrichment maps (EM)

5.3.1. Enrichment maps

The first conspicuous result for all enrichment maps is that there are no visible edges connecting the nodes indicating that all hallmark pathways from the Human Molecular Signatures Database are indeed summarized with, and assigned genes with minimum overlaps. Hallmark gene sets represent clearly defined pathways with minimum redundancy which makes it much easier to filter out biological processes impacted by different treatment conditions.

5.3.2. DAPT- GSEA, LEA, EM

The summary of GSEA results in the form of an enrichment map, for 2 µM DAPT treated Jurkat T-cell line is shown in Figure 19. There are two upregulated gene sets and one downregulated one according to the most stringent criterion of FWER p-value<0.05. Upregulated gene sets are involved in cholesterol homeostasis and MTORC1 signaling while the downregulated one is the Notch signaling gene set. Less restrictive and commonly taken criterion of nominal p-value<0.05 and FDR q-value<0.1, additional to the gene sets mentioned above, yields heme metabolism as upregulated and MYC targets V2 as downregulated gene sets.

Subsequent leading-edge analysis revealed the upregulation of HMGCS1 (3-hydroxy-3-methylglutaryl (HMG) Coenzyme A synthase) and CYP51A1 (Lanosterol 14-alpha demethylase) genes, both of which are involved in cholesterol homeostasis and MTORC1 signaling (*https://www.genenames.org/*, no date; *https://www.ncbi.nlm.nih.gov/gene/*, no date; *https://www.gsea-msigdb.org/gsea/msigdb*, no date).

Downregulated genes include HES1 (hes family bHLH transcription factor 1) and DTX1 (deltex E3 ubiquitin ligase 1) both of which are members of the Notch signaling pathway. (*https://www.genenames.org/*, no date; *https://www.ncbi.nlm.nih.gov/gene/*, no date; *https://www.gsea-msigdb.org/gsea/msigdb*, no date).
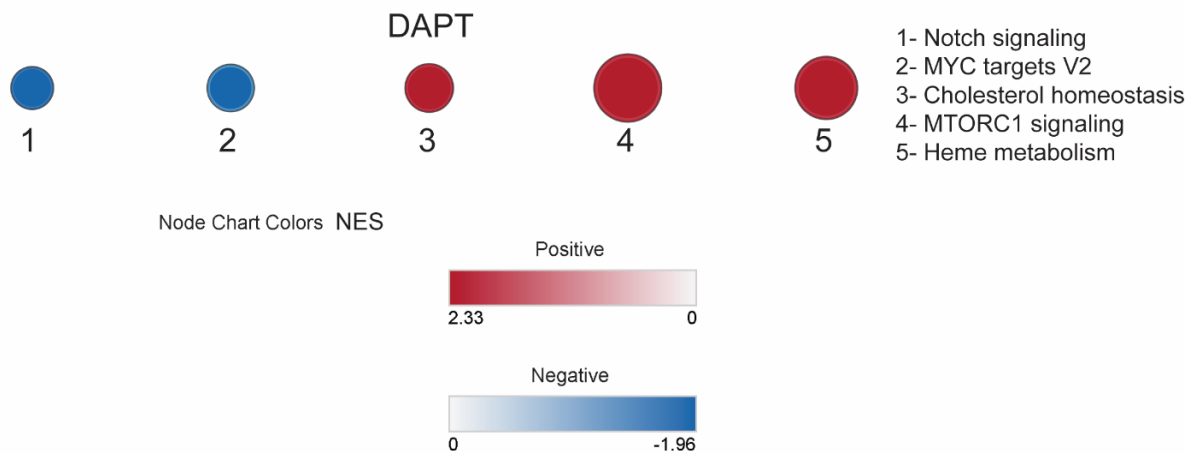
Figure 19. Enrichment map for 2 μM DAPT treated Jurkat T-cell line. Node size corresponds to the number of genes in a given gene set while color intensity represents the normalized enrichment score (NES) based on the legend shown in the figure. All gene sets shown are those that satisfy the nominal p<0.05 and FDR q<0.1 criterion.

5.3.3. RIN1- GSEA, LEA, EM

The summary of GSEA results in the form of an enrichment map, for 2 μM RIN1 treated Jurkat T-cell line is shown in Figure 20. Based on both criteria (nominal p value and FDR q value), there are no significantly upregulated gene sets. The FWER p-value<0.05 criterion gives only G2M checkpoint gene set as the significantly downregulated one. This is expanded by an additional 16 significantly downregulated gene sets given in Figure 20., should the second nominal p<0.05 and FDR q<0.1 criterion be taken into account.

Subsequent leading-edge analysis revealed the downregulation of several genes involved in multiple pathways. Those genes include but are not limited to, RHOB (ras homolog family member B) , GADD45B (growth arrest and DNA damage inducible beta), F3 (coagulation factor III, tissue factor), JUN (Jun proto-oncogene, AP-1 transcription factor subunit), MXD1 (MAX dimerization protein 1) , CLU (clusterin), TGFB1 (transforming growth factor beta 1), MMP2 (matrix metallopeptidase 2), SOCS1 (suppressor of cytokine signaling 1), C1R (complement C1r), NDRG1 (N-myc downstream regulated 1), IL2RB (interleukin 2 receptor subunit beta), CDKN1C (cyclin dependent kinase inhibitor 1C) and SLC6A8 (solute carrier family 6 member 8). Pathways they participate in are Ras pathway, NFkB pathway, MYC pathway, E2F pathway, JUN pathway, TGFβ pathway, IL2-STAT5 pathway, complement system, coagulation,

inflammatory response, apoptosis and p53 pathway (*https://www.genenames.org/*, no date; *https://www.ncbi.nlm.nih.gov/gene/*, no date; *https://www.gsea-msigdb.org/gsea/msigdb*, no date).
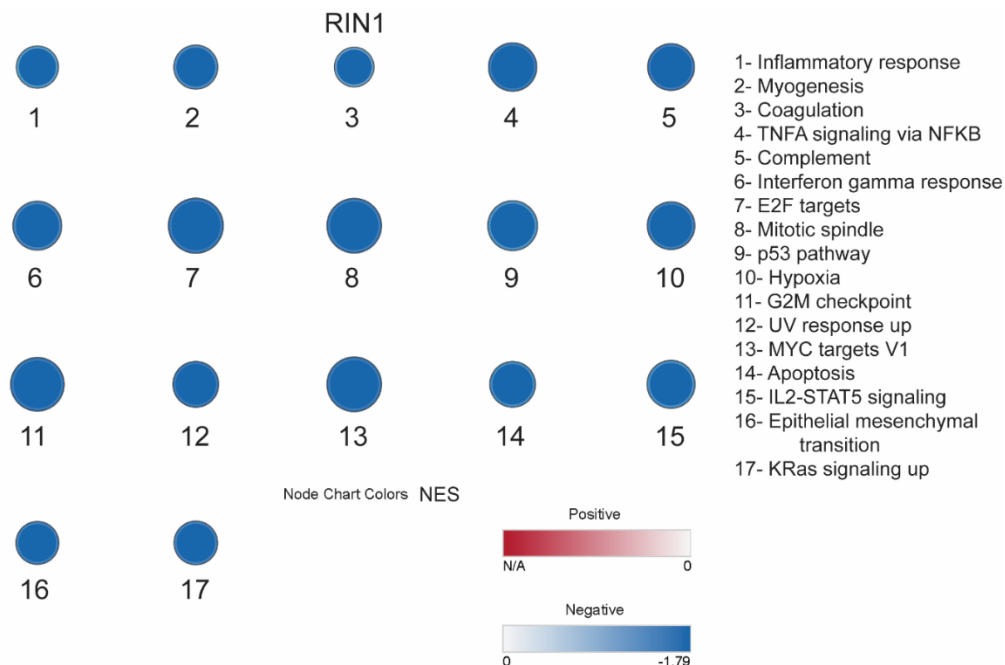

Figure 20. Enrichment map for 2 µM RIN1 treated Jurkat T-cell line. Node size corresponds to the number of genes in a given gene set while color intensity represents the normalized enrichment score (NES) based on the legend shown in the figure. All gene sets shown are those that satisfy the nominal p<0.05 and FDR q<0.1 criterion.

5.3.4. CB-103- GSEA, LEA, EM

The summary of GSEA results in the form of an enrichment map, for 10 µM CB-103 treated Jurkat T-cell line is shown in Figure 21. The most conservative criterion (FWER p<0.05) gives two significantly upregulated gene sets which are unfolded protein response and MTORC1 signaling gene sets. On the other hand, four gene sets are significantly downregulated, namely MYC targets V2, E2F targets, Notch signaling and apical surface gene sets. The less restrictive criterion (nom p<0.05 and FDR q<0.1) yields 8 more significantly upregulated and 3 more downregulated gene sets, as shown in Figure 21.

Subsequent leading-edge analysis revealed the upregulation of several genes involved in multiple pathways. Those genes include but are not limited to, ATF3 (activating transcription factor 3), PPP1R15A (protein phosphatase 1 regulatory subunit 15A), DDIT3 (DNA damage inducible transcript 3), SLC7A11 (solute

carrier family 7 member 11), TRIB3 (tribbles pseudokinase 3), VEGFA (vascular endothelial growth factor A), ASNS (asparagine synthetase (glutamine-hydrolyzing), GADD45A (growth arrest and DNA damage inducible alpha). Pathways that those genes participate in are cellular stress response, unfolded protein response, apoptosis, p53 response, p38/JNK pathway, C/EBP pathway, NFkB pathway, hypoxia pathway, MTORC1 pathway, Ras pathway, cholesterol homeostasis and heme metabolism (*https://www.genenames.org/*, no date; *https://www.ncbi.nlm.nih.gov/gene/*, no date; *https://www.gsea-msigdb.org/gsea/msigdb*, no date).

Downregulated genes include but are not limited to, LFNG (LFNG O-fucosylpeptide 3-beta-N-acetylglucosaminyltransferase), HES1 (hes family bHLH transcription factor 1), AKAP7 (A-kinase anchoring protein 7), SLC34A3 (solute carrier family 34 member 3). Pathways whose members those genes are, are Notch signaling pathway, Ras pathway and apical surface pathway (*https://www.genenames.org/*, no date; *https://www.ncbi.nlm.nih.gov/gene/*, no date; *https://www.gsea-msigdb.org/gsea/msigdb*, no date). Additional downregulated pathways whose genes aren't pinpointed in this results section due to their exclusive membership of a single pathway, are MYC pathway, E2F pathway and G2M checkpoint signaling pathway (*https://www.gsea-msigdb.org/gsea/msigdb*, no date).
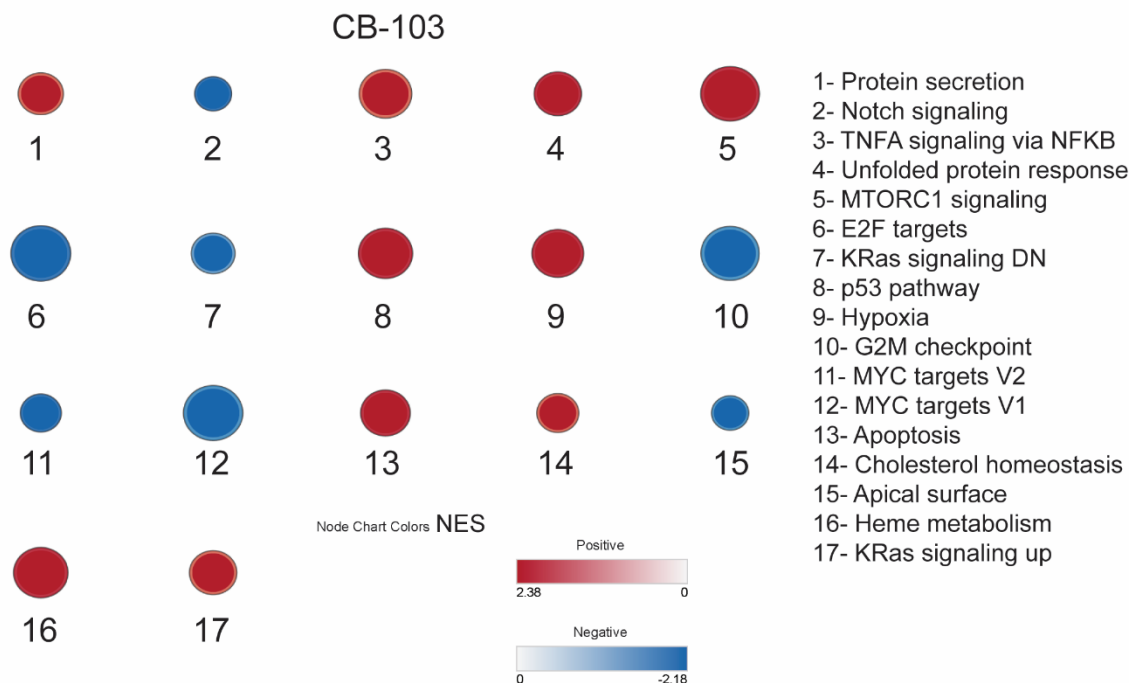
Figure 21. Enrichment map for 10 µM CB-103 treated Jurkat T-cell line. Node size corresponds to the number of genes in a given gene set while color intensity represents the normalized enrichment score (NES) based on the legend shown in the figure. All gene sets shown are those that satisfy the nominal p<0.05 and FDR q<0.1 criterion.

5.3.5. siRBPJ- GSEA, LEA, EM

The summary of GSEA results in the form of an enrichment map, for siRBPJ treated Jurkat T-cell line is shown in Figure 22. Based on FWER p<0.05 criterion, there are no significantly upregulated gene sets and MYC targets V1 is the only representative of significantly downregulated ones. If the second criterion is taken into account (nom p<0.05 and FDR q<0.1), the list of significantly downregulated genes is expanded to include the additional 5 gene sets as shown in Figure 22.

Subsequent leading-edge analysis revealed the downregulation of 4 genes. Those genes are VAMP3 (vesicle associated membrane protein 3), RBPJ (recombination signal binding protein for immunoglobulin kappa J region), FARP1 (FERM, ARH/RhoGEF and pleckstrin domain protein 1) and FGD4 (FYVE, RhoGEF and PH domain containing 4). Pathways those genes are responsible for, are protein secretion pathway, Notch signaling pathway, hypoxia pathway, mitotic spindle proteins and cytoskeleton proteins and its anchorage to the cell membrane (*https://www.genenames.org/*, no date; *https://www.ncbi.nlm.nih.gov/gene/*, no date; *https://www.gsea-msigdb.org/gsea/msigdb*, no date).

Figure 22. Enrichment map for siRBPJ treated Jurkat T-cell line. Node size corresponds to the number of genes in a given gene set while color intensity represents the normalized enrichment score (NES) based on the legend shown in the figure. All gene sets shown are those that satisfy the nominal p<0.05 and FDR q<0.1 criterion.
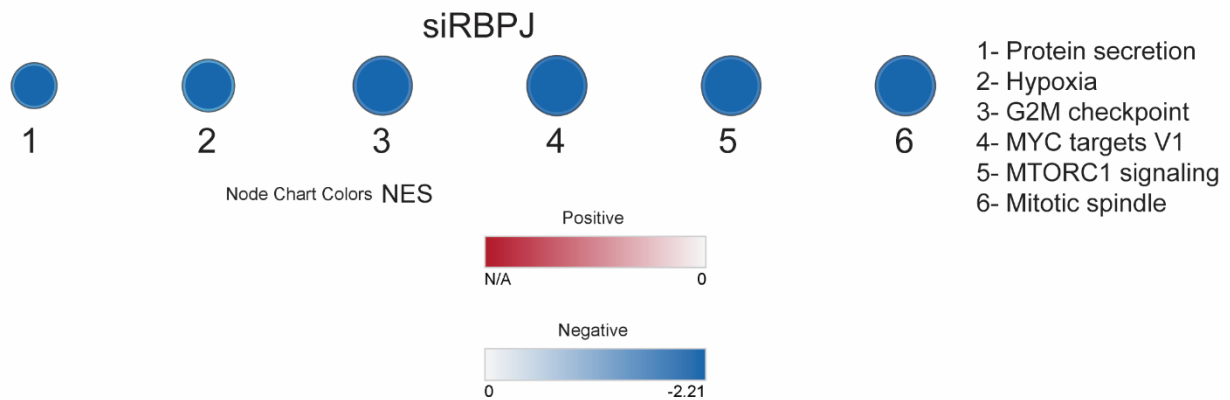
6. Discussion

6.1. Luciferase assays

Luciferase assay conducted on HeLa RBPJ KO#42 cell line transfected with NICD and RBPJ wild type constructs (together with luciferase reporter responsive to RBPJ) (Figure 4.), and treated with RIN1 and CB-103, shows the inhibition of relative luciferase activity compared to DMSO control, confirming the literature about the inhibition of RBPJ by those inhibitors (Hurtado *et al.*, 2019; Lehal *et al.*, 2020). The same observed inhibition holds true for RBPJ-VP16 construct (Figure 5.). To rule out the possibility that the inhibition could be based on additional Notch coactivators that interact with RBPJ, luciferase assay was conducted with RBPJ-VP16 Notch double mutant (Figure 6.) and mutant with five mutations (RBPJ-VP16-NBM) (Figure 7.). Both mutants harbor mutations in RBPJ which render them deficient for Notch cofactor binding. Despite the absence of Notch cofactor binding, there was still strong inhibition of relative luciferase activity indicating inhibition of the respective RBPJ-VP16 mutant fusion proteins. This inhibition could in theory be based on the inhibition of RBPJ DNA-binding, inhibition of VP16's transactivation capability or the inhibition of luciferase enzyme itself.

Therefore, the next step was to assess Gal4-VP16 fusion protein (with luciferase construct under Gal4 responsive element) which was again inhibited by both RIN1 and CB-103 (Figure 8.). This opens even more questions rather than answering them as now one could argue that on top of RBPJ and VP-16, Gal4 DNA-binding could also be inhibited. This might be an unusual result in a way that RIN1 supposedly has quite significant off-target effects. Therefore, to make sure that the inhibition is not an artifact based on an uneven cell number and different transfection efficiency, dual Firefly-Renilla luciferase assay was performed on Gal4-VP16 construct. In this scenario, Renilla luciferase was constitutively expressed under the thymidine kinase promoter and served as an internal control. No statistically significant inhibition could be observed for Renilla luciferase when looked at on its own, in either case of inhibitors (Figure 10.). This indicated that neither RIN1 nor CB-103 act as inhibitors of Renilla luciferase enzyme and confirmed similar transfection efficiency for all treatment conditions. However, the relative Firefly to Renilla luciferase activity was significantly inhibited by both inhibitors (Figure 9.). This leaves the previous question open and means that they either truly inhibit Gal4-VP16 construct or the firefly luciferase enzyme itself.

To test the latter hypothesis, luciferase assay was performed on constitutively expressed Firefly luciferase under the Simian virus 40 promoter (Figure 11.). The results showed a very strong, concentration dependent progressive inhibition in case of CB-103 confirming that it inhibits the luciferase enzyme itself. CB-103 was therefore left out at this stage and not tested in further experiments. Despite inhibiting the luciferase enzyme itself, it remains elusive whether CB-103 might also act as an inhibitor of RBPJ DNA-binding,

Gal4 DNA-binding or VP16's transactivation capability. RIN1 on the other hand showed the inhibition of Firefly luciferase enzyme only in case of the highest 10 µM concentration and so additional experiments were performed to try to elucidate the basis of previous series of inhibitions.

To check for RIN1's potential to inhibit Gal4 DNA-binding, Gal4-p65 assay was performed in which p65 was used as an alternative transactivator (Figure 12.). There was a strong concentration dependent progressive inhibition of Gal4-p65 fusion protein opening even more questions by including p65 as an additional potential inhibitory target of RIN1. Next experiment aimed to check for the inhibition of p65 which, if not inhibited, would mean that Gal4-p65 inhibition was actually based on the inhibition of Gal4 DNA-binding. To test this hypothesis, p65 as a transactivator on its own was used in an experiment where luciferase enzyme was placed under the 3xNFκB promoter containing the p65 responsive element (Figure 14.). The results showed no significant inhibition apart from the highest concentration of RIN1 (10 µM) which was expected as this same concentration inhibits the Firefly luciferase enzyme itself. The aforementioned means that Gal4-p65 inhibition is based on the inhibition of Gal4 DNA-binding rather than p65's transactivation capability. Coming back to Gal4-VP16 construct, it now becomes clear that the inhibition is based on Gal4 DNA-binding but the question that ensues is whether simultaneous inhibition of VP-16 is possible.

To further test this hypothesis, a VP-16 construct with a different DNA-binding domain was employed, namely HNF6-VP16 (Figure 15.). This construct again showed a very strong statistically significant and concentration dependent progressive inhibition by RIN1. Consequently, the aim of the next assay was to test HNF6 on its own as it can also act independently as a transcriptional activator (Figure 16.). The highest RIN1 concentration (10 µM) exhibited a very strong inhibition which is as expected since it inhibits the luciferase enzyme itself. Moreover, there was a significant inhibition by 5 µM concentration. What is rather interesting was the lack of significant inhibition for the lowest 2.5 µM concentration. Concerning this result, what comes to the fore is that RIN1 acts as an inhibitor of HNF6 DNA binding but the lowest tested concentration of 2.5 µM was not high enough to induce this effect. This result showed that the interference with HNF6 DNA-binding is responsible for HNF6-VP16 construct's inhibition but what remains unclear is if VP16 could be inhibited on its own.

6.2. Immunofluorescence assay

Immunofluorescence assay was carried out on HeLa wild type cells to test whether RIN1 and CB-103 might interfere with RBPJ's subcellular localization. This could be achieved by either inhibition of nuclear import or enhanced nuclear export by RITA protein which could consequently act as a negative regulator. The immunofluorescence assay confirmed there was no interference with the subcellular localization of RBPJ

which was localized within the nucleus for all tested concentrations of both RIN1 (2.5 µM, 10 µM), CB-103 (10 µM, 40 µM) as well as DMSO solvent control (Figures 17. and 18.).

6.3. Gene Set Enrichment Analysis (GSEA) and Leading-edge analysis (LEA)

The results of GSEA and leading-edge analysis for DAPT, RIN1, CB-103 and siRBPJ-treated Jurkat T-cell line showed the significant downregulation of the Notch signaling pathway as a whole, in case of DAPT (Figure 19.) and CB-103 (Figure 21.). However, RIN1 (Figure 20.) and siRBPJ (Figure 22.) treated cells failed to exhibit the same result. Nevertheless, siRBPJ, as expected, leads to the downregulation of RBPJ's expression even though this effect is not sufficient to lead to a significant change in the expression levels of Notch signaling pathway as a whole. RIN1 on the other hand does not lead to a significant change in expression of any core enrichment genes belonging to the Notch signaling pathway. This might seem contradictory at first, given the results of Hurtado et al. 2019 who showed that RIN1 has similar effects to siRBPJ in a way that it significantly upregulates HES1, HES5 and DTX1 compared to CB-103 and DAPT which downregulate them. Notwithstanding, observations of GSEA, and single gene differential expression as calculated by DESeq2 algorithm from RNA sequencing data and confirmed by qPCR are valid and in line with each other. One should keep in mind that qPCR and DESeq2 are methods that look upon genes as isolated entities while GSEA looks at the entire pathway and whether genes belonging to the given pathway as a whole, are differentially expressed. Therefore, GSEA can identify the whole set of related genes as differentially expressed and even more so core enrichment genes of a given set, even though the individual genes of the set don't necessarily have to be differentially expressed and vice versa. This has biological implications as moderate, statistically significant changes in related genes with similar biological function can have more impact on the cell and ultimately organism than multifold changes in single genes (Subramanian *et al.*, 2005). Moreover, unlike DAPT and siRBPJ which seem to have narrow and highly specific effects in terms of differentially expressed pathways, RIN1 and CB-103 tend to have a much broader impact by leading to upregulation or downregulation of more than a dozen of pathways. Whether this is due to the lack of their specificity, and potential off-target effects or crosstalk between the Notch signaling pathway and other involved upregulated or downregulated pathways remains to be seen.

Concerning the aforementioned, the next section of this discussion is dedicated to the crosstalk between the Notch signaling pathway and other pathways identified as significant by GSEA. Finally, pathways up- or downregulated by each inhibitor are put within the context of a crosstalk.

6.3.1. PI3K/Akt and mTOR signaling pathways and their crosstalk with the Notch pathway

Studies had shown that the activated Notch target gene *Hes1* directly represses PTEN (Bailis and Pear, 2012) whose substrate is the lipid phosphatidylinositol-3,4,5-triphosphate (Porta, Paglino and Mosca, 2014). PTEN otherwise inhibits the PI3K/AKT signaling pathway but through Hes1 mediated PTEN repression, PI3K remains active after growth factor binding to receptor tyrosine kinases which through their autophosphorylation leads to recruitment of PI3K. PI3K can then phosphorylate phosphatidylinositol-4,5-bisphosphate leading to the production of phosphatidylinositol-3,4,5-triphosphate which in turn recruits and activates PDK1 and AKT/PKB. AKT acts upon multiple target proteins involved in cell survival, cell growth and cell cycle progression (Porta, Paglino and Mosca, 2014). Notable AKT effects which can be in principle induced in case of the active Notch signaling are inhibition of proapoptotic factors Bad and Pro-caspase 9 which prevents apoptosis; activation of MDM2 ubiquitin ligase which targets p53 for proteasomal degradation preventing the cell-cycle arrest and apoptosis in case of DNA damage repair; inactivation of GSK3-β which upregulates Cyclin D1 leading to increased progression through G1/S checkpoint (Porta, Paglino and Mosca, 2014); and activation of NFκB which is involved in immunity, apoptosis and differentiation (Oeckinghaus, Hayden and Ghosh, 2011).

Moreover, hyperactivation of the Notch signaling was shown to increase the protein expression level of raptor and the assembly of mTORC1 complex therefore contributing to the mTORC1 signaling (Shimobayashi and Hall, 2014). The link between the PI3K/AKT and mTOR signaling pathways is through AKT which inhibits TSC2 subunit from TSC2/TSC1 complex alleviating inhibition of Rheb GTP and leading to increased activation of mTORC1 complex (Porta, Paglino and Mosca, 2014; Zou *et al.*, 2020). mTOR signaling pathway has two main distinct complexes, namely mTORC1 and mTORC2. mTORC1 is composed of mTOR/raptor/GβL/deptor and is responsible for cell growth and metabolism while mTORC2 comprises mTOR/rictor/GβL/PRR5/deptor and regulates proliferation and survival (Zou *et al.*, 2020). Therefore, active Notch signaling, on top of activating AKT which results in increased activity of mTORC1, also activates mTORC1 complex directly through increasing the expression of raptor. Active mTORC1 in turn activates S6K (ribosomal S6 kinase) and inhibits 4EBP1 (eIF4E-binding protein 1) which activates the protein synthesis (Shimobayashi and Hall, 2014).

6.3.2. MYC signaling pathway and its crosstalk with the Notch pathway

Studies had also shown that the mouse *c-myc* promoter has Notch1 responsive regulatory elements and discovered the interaction between Notch1 and *c-Myc*. This was later confirmed in T-cell acute lymphoblastic leukemia where it was shown that Notch1 directly induces the expression of c-MYC (Palomero *et al.*, 2006; Weng *et al.*, 2006). However, Notch1 is responsible for only a fraction of c-MYC

expression which is controlled by further upstream regulatory factors (Palomero *et al.*, 2006). The MYC signaling pathway plays a role in regulating the cell cycle, DNA replication and metabolism (Sanchez-Martin and Ferrando, 2017). The MYC protein itself is a proto-oncogene which when dysregulated (constitutive expression due to amplification or loss of upstream regulators), is involved in a variety of cancers (Dang, 2012). MYC exerts its function in cooperation with Max by forming a heterodimer that binds to E-box motif in the DNA. However, the same motif can be bound by other transcription factors such as SREBP, HIF-1, NRF1 and ChREBP which are involved in the metabolism of cholesterol and fatty acids, angiogenesis, mitochondrial respiration and biogenesis, and carbohydrate metabolism, respectively (Dang, 2012). What is worth noting is that MYC activates microRNA, miR-17 cluster which inhibits PTEN leading to increased activity of PI3K/AKT pathway; inhibits proapoptotic BimL protein which prevents apoptosis; and inhibits E2F signaling disrupting the DNA damage control (Dang, 2012).

Having said that, there is a link between the Notch, MYC and PI3K/AKT pathway in a way that the Notch signaling, in particular Notch1 directly induces the expression of MYC which induces miR-17 which in turn inhibits PTEN leading to increased activity of PI3K/AKT pathway which activates mTORC1 through inhibiting TSC2. On top of that, Notch1 can directly repress PTEN by upregulating the expression of Hes1, therefore amplifying the effect of MYC induced PI3K/AKT activation.

6.3.3. MAPK signaling pathway and its crosstalk with the Notch pathway

MAPK signaling pathway is the mitogen-activated protein kinase signaling pathway that is responsible for regulating the stress response, proliferation, apoptosis and differentiation. It includes a basic layer of three kinases that follow a phosphorylation cascade, which can be expanded by additional two kinases in variations of the pathway. Four main MAPK pathways exist which are named based on the components of kinase layers- ERK1/2 pathway, c-Jun N-terminal kinase (JNK), p38 MAPK and ERK5. JNK and p38 pathway are involved in the stress response and apoptosis while ERK5 and the best studied ERK1/2 play a role in the cell proliferation and differentiation (Guo *et al.*, 2020).

Notch and MAPK signaling pathway were also shown to be closely linked in a newly proposed extended mechanism of action. However, the study was conducted on *Drosophila* and so caution is necessary while interpreting the results within the context of a human cell line such as Jurkat T-cell line. While similar types of interactions might be present in mammals, this can't be definitely stated. Previously, it had been identified that active Notch signaling, in the majority of cases, leads to the cells remaining in the undifferentiated state while MAPK induces the differentiation. Therefore, Notch and MAPK have the opposing effects on the cell fate. However, the study employing microarrays on *Drosophila* embryos showed that the active Notch signaling modulates and respecifies the Ras signaling output whereby some Ras targets show no change

while the others show an altered response. The other way around also holds true, active Ras signaling also respecifies the Notch output but not to such a pronounced extent. Namely, authors found out that 65% of Ras targets also respond to Notch activation (Hurlbut, Kankel and Artavanis-Tsakonas, 2008). Some pinpointed genes that responded to concurrent activation of Notch and Ras were Gap1 and Mkp3, both of which are negative Ras regulators, and Fringe enzyme which acts positively on Notch signaling by increasing the sensitivity of Notch receptor to Delta ligand. On the other hand, Ras genes regulated by Notch upon its separate activation were RTK ligand spitz; rhomboid and star (regulate the spitz processing), RTK receptors heartless, breathless and EGFR as well as the three genes already mentioned above (Hurlbut, Kankel and Artavanis-Tsakonas, 2008). Moreover, it had been shown in *Drosophila* imaginal epithelium experiments aiming to elucidate tumor heterogeneity-driven cancer progression, that benign tumors of Ras and Src interact with each other at an interface which promotes invasiveness. Ras benign tumor cells upregulated Delta ligand while Src benign tumor cells upregulated Notch receptor. Activated Notch signaling in Src cells lead to the downregulation of E-cadherin via Zfh1/ZEB1 repressor, and upregulation of the cytokine Unpaired/IL-6 which in turn activated JAK-STAT signaling in Ras tumor cells. This eventually led to the downregulation of E-cadherin promoting invasiveness (Enomoto, Takemoto and Igaki, 2021). Those studies had shown that there are genes that additively respond to Notch and Ras signaling as opposed to the antagonistic paradigm that previously prevailed.

Briefly, it had been shown in *Drosophila* that the active Notch signaling can induce Gap1 and Mkp3 genes which act as suppressors of Ras signaling therefore inhibiting the differentiation. Mechanistically, with regards to ERK1/2 pathway, growth factor activated RTK, after autophosphorylation, recruit Grb2 to the cell membrane. Grb2 is associated with SOS protein which is a guanine nucleotide exchange factor that replaces GDP with GTP, on Ras, which leads to its activation. Active GTP bound Ras then stimulates the kinase Raf which phosphorylates and activates MEK 1/2 (MAPK/ERK kinase 1/2) that in turn phosphorylates and activates ERK1/2. ERK1/2 subsequently activates a broad spectrum of other effectors regulating the cellular proliferation and differentiation (Aksamitiene, Kiyatkin and Kholodenko, 2012). Gap1 dephosphorylates GTP on Ras turning it into an inactive RasGDP state (Rudack *et al.*, 2012) while Mkp3 binds to and dephosphorylates ERK also leading to its inactivation (Kim *et al.*, 2004). On the other hand, Ras signaling can upregulate the Delta ligand and promote the Notch signaling.

ERK1/2 signaling pathway shows an extensive crosstalk with PI3K/AKT pathway and vice-versa. PI3K's formation of phosphatidylinositol-3,4,5-triphosphate leads to recruitment of scaffolding proteins GAB, IRS and Grb7 which are subsequently phosphorylated and can interact with a variety of other molecules including ERK, STAT3 and STAT5. Furthermore, GAB can recruit Grb2-SOS which results in the activation

of Ras. Moreover, GAB1 can associate with SHP2 increasing its phosphatase activity leading to dephosphorylation of RasGAP which also promotes Ras activation. PI3K can also stimulate Raf and MEK (Aksamitiene, Kiyatkin and Kholodenko, 2012). Despite PI3K's promoting role in ERK signaling, PI3K's downstream effectors, namely Akt and mTOR have inhibitory effect on ERK signaling. Most notably, Akt can phosphorylate Raf which prevents its association with the membrane and consequently its activation. ERK pathway can also influence the activity of PI3K/Akt pathway through phosphorylation of GAB1 which depending on the residue, can either be stimulatory or repressive. ERK can phosphorylate and inhibit GSK3 which is a negative regulator of PTEN. This results in increased activity of PTEN which inhibits PI3K/Akt pathway. What is more, RasGTP can directly activate PI3K therefore creating a stimulatory effect on PI3K/Akt pathway (Aksamitiene, Kiyatkin and Kholodenko, 2012).

The Notch signaling can depending on the cellular context, environment and signal integration influence the Ras and PI3K/AKT crosstalk. In principle, it could activate PI3K through inhibition of PTEN. Subsequently, through mechanisms described above, Ras, Raf and MEK could become activated. Consequently, ERK activation can then in a negative feedback loop inhibit the activation of PI3K through activating PTEN by inhibiting its inhibitor. On the other hand, increased activation of AKT could also lead to the inhibition of Raf.

6.3.4. NFκB signaling pathway and its crosstalk with the Notch pathway

One of the most complex, intertwined and extensive crosstalks is perhaps that between the Notch and Nuclear factor kappa B (NFκB) signaling pathways (Osipo *et al.*, 2008). NFκB signaling pathway is represented by transcription factors implicated in the immune response and inflammation, proliferation, survival and differentiation. The main effectors are NFκB homo- or heterodimers, inhibitors of NFκB- IκB, and inhibitor of NFκB kinases-IKK. There are altogether five monomers that can form dimers with different binding affinities and transactivation capabilities- p50, p52, p65/RelA, RelB and cRel. They are regulated by 3 main pathways- canonical NFκB pathway, non-canonical NFκB pathway and alternative activation pathway (Mitchell, Vargas and Hoffmann, 2016).

The canonical NFκB signaling pathway is regulated by IKK1, IKK2 and NEMO (IKKγ) that form a protein complex which can be activated by either trans-autophosphorylation of IKK1/2 subunits brought into proximity by NEMO, phosphorylation of IKK1/2 subunits by upstream kinases such as TAK1, or by ubiquitination of NEMO. IKK1/2/NEMO complex activating signals include various inflammatory cytokines such as IL-1, TNF-α and pathogen-associated molecular patterns. Activated IKK1/2/NEMO complex binds to and phosphorylates IκB proteins (IκBα/β/ε complex together with p100) resulting in their ubiquitin-mediated proteasomal degradation. Upon IκB degradation, NFκB dimers (the most common one

being p50/RelA) are free from being bound by IκB, translocate into the nucleus and bind to NFκB responsive elements exerting their function (Mitchell, Vargas and Hoffmann, 2016). Signals activating the non-canonical NFκB pathway are developmental ones coming from TNF receptors such CD40, RANK, TNFR2, BAFFR and Fn14. Non-canonical pathway is mediated by NIK which substitutes the activity of NEMO, and IKK1. Unlike phosphorylation in the canonical pathway, signal transduction in the non-canonical pathway is enabled through stabilization and accumulation of NIK kinase which is, in the absence of signals, degraded by TRAF-cIAP complex. NIK then phosphorylates and activates IKK1 which phosphorylates p100 leading to its processing into p52 that dimerizes with RelB. The heterodimer complex, also known as NFκB2, then translocates into the nucleus where it activates the non-canonical NFκB gene expression pattern (Mitchell, Vargas and Hoffmann, 2016). Alternative NFκB pathway is activated by ribotoxic, genotoxic or shear stress and eventually involves the phosphorylation and degradation of IκBα (Mitchell, Vargas and Hoffmann, 2016).

The Notch signaling pathway was shown in Jurkat T-acute lymphoblastic leukemia cell line to induce the expression of p100 which can, as a part of IκB, inhibit the non-canonical NFκB pathway. However, p100, in its cleaved form p52 can in turn activate the pathway. Research on mouse hematopoietic precursors have shown that Notch signaling can also upregulate the expression of p50, p65, RelB and c-Rel therefore positively regulating the NFκB signaling pathway (Osipo *et al.*, 2008). The other way around, it was shown in B cells that p50/p65 can upregulate the expression of Notch target genes *Jagged1*, *HES5* and *Deltex1*. There are also physical interactions between the two pathways. In Jurkat T-cell line, it was shown that low levels of Notch1 intracellular domain can stimulate the NFκB signaling pathway by physically interacting with p50 while high levels inhibit the pathway. As this study used the overexpressed Notch1 intracellular domain, in case of high concentration, the interaction was predominantly nuclear and had a sequestering manner of action (Osipo *et al.*, 2008). Moreover, it had been reported that in CaSki cells, Notch1 can associate with IKK1 stimulating its kinase activity leading to proteasomal degradation of IκB proteins. Another novel mechanism of action involves Notch1/IKK1 complex's gene expression transactivation ability. Namely, it was previously shown that IKK1 can derepress the transcription of NFκB genes through chromatin remodeling by e.g. phosphorylation of H3 histone or SMRT corepressor. Therefore, Notch1 modulates IKK1's chromatin remodeling activity in a positive manner (Song *et al.*, 2008). Yet another study on T-cell acute lymphoblastic leukemia showed that HES1 which is a direct Notch target gene, represses CYLD deubiquitinase which is a negative regulator of IKK. This leads to increased activity of IKK which results in proteasomal degradation of IκB and enhanced canonical NFκB signaling. Conversely, the knockdown of Hes1 expression led to increased levels of CYLD and decreased NFκB signaling (Espinosa *et al.*, 2010).

To summarize, active Notch signaling can induce the expression of p50, p65, RelB and c-Rel therefore increasing the activity of NFκB pathway. Moreover, Notch1 can associate with IKK1 increasing its kinase activity and upregulating the NFκB signaling pathway. Conversely, canonical NFκB signaling pathway can upregulate the expression of Notch target genes *Jagged1*, *HES5* and *Deltex1*.

6.3.5. Hypoxia pathway and its crosstalk with the Notch pathway

Hypoxia pathway is activated under hypoxic conditions and is important for organism's adaptation to variable oxygen levels. It regulates a broad spectrum of signaling pathways including proliferation, survival, apoptosis, cellular metabolism, inflammation, hematopoiesis, angiogenesis, migration and epithelial mesenchymal transition (Wielockx *et al.*, 2019; Guo *et al.*, 2023). The main players in hypoxia pathway are hypoxia-inducible factors (HIFs) which belong to a family of basic helix-loop-helix transcription factors. They recognize the hypoxia response elements (HREs) in DNA therefore activating the transcription of their target genes (Wielockx *et al.*, 2019). HIFs are heterodimers composed of an α subunit which is an oxygen sensitive subunit whose expression is regulated based on oxygen levels, and a β subunit which is constitutively expressed. There are three main forms of the α subunit (Jing *et al.*, 2019). HIF1α is ubiquitously expressed, HIF2α is specific to and characteristic of certain cells like hematopoietic ones, adipocytes and glial cells, while very little is known about HIF3α (Jing *et al.*, 2019; Wielockx *et al.*, 2019). There are two main ways of HIFα inactivation under normoxic conditions. It is either hydroxylated at an asparagine residue by the factor inhibiting HIF (FIH) enzyme which prevents its binding to p300/CBP and consequently prevents the transcriptional activation; or it is hydroxylated at two proline residues by HIF prolyl hydroxylase domain (PHDs) which results in its ubiquitination via the von Hippel-Lindau tumor suppressor protein (pVHL) and subsequent proteasomal degradation. The substrates required for pVHL's function are oxygen, Fe(II), ascorbate and 2-oxoglutarate meaning that pVHL are less functional under hypoxic conditions due to the lack of oxygen as their substrate, which results in higher stability of HIFα subunit (Wielockx *et al.*, 2019).

Hypoxia and Notch signaling pathway also show an extensive and complex network of interactions (Guo *et al.*, 2023). Hypoxia pathway can directly activate the Notch signaling pathway through HIF1α which can bind to and stabilize NICD which results in the activation of *Hes* and *Hey* target genes. Moreover, HIF1α was also found to be recruited to the *Hey2* promoter, and to directly interact with and upregulate the activity of γ-secretase (Guo *et al.*, 2023). Notch can also upregulate the hypoxia pathway by upregulating the expression of HIF2α. Finally, there is an intertwined interaction between the Notch and hypoxia pathway mediated by FIH-1 whose substrates are both Notch intracellular domain and HIF1α. FIH-1 was shown to

have a higher affinity to NICD than HIF1α which could, in principle, lead to sequestration of FIH-1 by NICD in case of increased Notch signaling, and therefore, the lower activity of FIH 1 upon HIF1α. This would in turn stabilize HIF1α and increase the hypoxia signaling (Guo *et al.*, 2023).

In conclusion, the active Notch signaling pathway can upregulate the hypoxia pathway through NICD's sequestration of FIH or by upregulating the expression of HIF2α. Additionally, the hypoxia pathway can upregulate the Notch signaling pathway through HIF1α which can bind to and stabilize NICD or increase the activity of γ-secretase.

6.3.6. Cell cycle, p53 pathway and apoptosis and their crosstalk with the Notch pathway

The progression through cell cycle and proliferation in animal cells is primarily regulated by the presence of growth factors which allow the progression through G1 restriction point. Once this restriction point is passed, the cell is bound to progress through the entire cell cycle if all events necessary for progression had been completed successfully and correctly which is in turn controlled by cell cycle checkpoints. Cells have 4 main cell cycle checkpoints that ensure no aberrant division takes place. Those are G1, S and G2 checkpoints also deemed DNA damage checkpoints and the M phase checkpoint also known as the spindle assembly checkpoint. Key proteins regulating the progression through the cell cycle checkpoints are cyclins (Cycs), cyclin-dependent kinases (Cdks) and cyclin-dependent kinase inhibitors (CKIs) of the p21 and the p16 family (Cooper, 2019).

The Notch intracellular domain was reported to directly induce the expression Cyclin D1 through RBPJ-dependent binding to Cyclin D1 promoter, and to activate Cdk2. This alone is not sufficient to drive the malignant transformation but is rather one of the contributing factors together with other mutations and aberrations (Ronchini and Capobianco, 2001). Another study on leukemic T-cells identified Cyclin D3 as the direct target of Notch intracellular domain whereby NICD-RBPJ-MAML complex was shown to bind to Cyclin D3 promoter. However, NFκB subunit p50 binds the same promoter and enhances the activity of Notch driven activation. Moreover, it was indirectly through GSI mediated abrogation of Cdk4 and Cdk6's activity, shown that the Notch can increase the expression of Cdk4 and Cdk6 as well as phosphorylation of Rb protein but the exact mechanism still remains elusive (Joshi *et al.*, 2009). Concerning the interaction between the Notch and p53, Notch can downregulate the expression of INK4a/ARF tumor suppressor, which otherwise when active, acts as an inhibitor of Mdm2 E3 ubiquitin-ligase whose activity results in the degradation of p53. Therefore, active Notch signaling leads to degradation of p53 by inhibiting the inhibitor

of Mdm2 which in turn leads to decreased apoptosis and increased cell survival (Reichrath and Reichrath, 2021).

In summary, the Notch intracellular domain can directly induce the expression of Cyclin D1 and D3, as well as activate Cdk2. It can also likely but through a yet unknown mechanism induce the expression of Cdk4 and Cdk6, and phosphorylate the Rb protein. Moreover, the Notch signaling pathway can downregulate the expression of Mdm2's inhibitor resulting in the degradation of p53 and decreased apoptosis. All of the mentioned mechanisms of action promote the cell cycle progression while inhibiting the apoptosis.

6.4. The effects of siRBPJ, RIN1, CB-103 and DAPT treatment in Jurkat cells on the crosstalk between the Notch and other signaling pathways

The siRBPJ-treated Jurkat cell line serves as a control for integration between the Notch and other signaling pathways in case of RBPJ's knockdown. Comparably, similar results are expected concerning pathway up- or downregulation in case of RIN1 and CB-103 if they indeed act specifically on RBPJ. However, the inhibitor effects also depend on the level and state of Notch signaling at the time of RBPJ's inhibition. If Notch signaling pathway is 'off', RBPJ knockdown can lead to derepression of the target genes. Conversely, if the Notch pathway is maximally 'on', the loss of RBPJ can lead to downregulation of the target genes. Also, if e.g. RIN1 inhibits RBPJ/SHARP interaction more than CB-103, completely different effects could be achieved. Therefore, caution is necessary while interpreting the GSEA results.

While siRBPJ (Figure 22.) did not lead to a significant downregulation of the Notch signaling pathway as a whole, it did significantly and highly knockdown the expression of RBPJ (log2(fold change)= -1.93 and padj= $1.63*10^{-27}$). However, the pattern of downregulated hallmark gene sets points out to the possibility of RBPJ's knockdown influencing the other pathways in a manner consistent with the Notch pathway downregulation. In particular, MYC, mTORC1 and hypoxia pathway downregulation is consistent with the notion of downregulated Notch pathway as a whole.

RIN1 (Figure 20.) in much the same manner does not lead to a significant downregulation of the Notch signaling pathway but some parts of the other pathways downregulation pattern, at least concerning MYC, hypoxia and NFκB, is similar to what is expected in case of downregulated Notch signaling. What might seem inconsistent with the Notch pathway downregulation is the downregulation of p53 pathway, apoptosis and E2F targets pathway which are supposed to be downregulated in case of the active Notch signaling. This points out to a much more complex and intertwined network of pathway integration than what might

be currently known. Even more so, RIN1's impact on the signaling pathways changes is much more pronounced and broader than that of siRBPJ, likely signifying the off-target effects.

Much like RIN1, CB-103 (Figure 21.) has a broader and more complex effects on changes in signaling pathways than siRBPJ. It is worth emphasizing that the Notch signaling pathway as a whole is downregulated indicating a slightly different CB-103's mode of action than that of RIN1. The very reason behind it still remains inconclusive as not enough data is available. Consistent with the Notch pathway downregulation, MYC pathway is also downregulated while p53 and apoptosis are upregulated. However, the same does not hold true for mTORC1, hypoxia and NFκB which, based on the literature, should also be downregulated. Moreover, Ras pathway upregulation is in line with the literature. It is worth pointing out that the apical surface proteins responsible amongst others for the integrity of the cell membrane are downregulated which explains some of the unpublished results from Prof. Dr. Oswald's work group. Namely, light microscope photos of HeLa wild type cells treated with varying concentrations of CB-103 taken by me show the 'inflated bubble-like' cell membrane forming a fine and delicate structure like a cape around the cell.

DAPT-treated Jurkat cells (Figure 19.) exhibit the downregulation of entire Notch signaling pathway which is in line with the literature. Surprisingly, only a handful of other signaling pathways are affected making DAPT resemble siRBPJ treatment condition more than RIN1 or CB-103. As DAPT is a gamma secretase inhibitor which is in turn involved in the cleavage of a large number of other proteins involved in different pathways, one might expect a broader impact on the multiple pathways which is rather not the case. MYC pathway is downregulated which is in agreement with the literature while mTORC1 pathway is upregulated which does not directly conform to the literature. This again points out that a much more complex pathway integration is taking place than what might be known from the literature.

In summary, siRBPJ and RIN1 didn't result in the statistically significant downregulation of the Notch signaling pathway as a whole. Nevertheless, the pattern of gene set expression changes is to an extent similar to what one might expect in case of downregulated Notch pathway. DAPT led to downregulation of the Notch signaling pathway as a whole but the impact on other gene sets is much more narrow than expected at first, given the broadness of γ-secretase substrates. CB-103 also significantly downregulated the Notch pathway as a whole but resembled more RIN1 concerning the wide pattern of gene set expression changes. However, individual changes (up- vs downregulation) differ between the two inhibitors, signifying a slightly different mode of action.

7. Conclusions

RIN1, and CB-103 which was used as a positive control, are a novel class of Notch signaling pathway inhibitors also known as transcription blockers which target the ternary NICD-RBPJ-MAML activation complex. This study provides a more detailed insight into their molecular mechanisms of action through luciferase assays and immunofluorescence as well as the broader cellular context of the gene expression changes induced by inhibitor treatment, as analyzed by Gene Set Enrichment Analysis.

The conclusions of the study are as follows:

1. CB-103 led to the inhibition of the Firefly luciferase enzyme itself while Renilla used as an internal control wasn't affected. What remains open is whether CB-103 can furthermore inhibit RBPJ DNA-binding, Gal4 DNA-binding and/or VP16's transactivation capability.
2. RIN1 exhibited the conclusive inhibition of Gal4 DNA-binding and HNF6 DNA-binding while p65's transactivation capability wasn't affected. What remains elusive is whether VP16, on its own, could be inhibited too.
3. Neither RIN1 nor CB-103 did interfere with the nuclear localization of the transcription factor RBPJ.
4. Both RIN1 and CB-103 exhibited a much broader pattern in gene expression changes compared to siRBPJ which indicates a less specific mode of action and more elaborate signal integration pathways than what is currently known from the literature.

8. References

Aksamitiene, E., Kiyatkin, A. and Kholodenko, B.N. (2012) 'Cross-talk between mitogenic Ras/MAPK and survival PI3K/Akt pathways: A fine balance', *Biochemical Society Transactions*, pp. 139–146. Available at: https://doi.org/10.1042/BST20110609.

Aster, J.C., Pear, W.S. and Blacklow, S.C. (2017) 'The Varied Roles of Notch in Cancer', *Annual Review of Pathology: Mechanisms of Disease*, 12(1), pp. 245–275. Available at: https://doi.org/10.1146/annurev-pathol-052016-100127.

Bailis, W. and Pear, W.S. (2012) 'Notch and PI3K: how is the road traveled?', *Blood*, 120(7), pp. 1349–1350. Available at: https://doi.org/10.1182/blood-2012-06-435099.

Carter, M. and Shieh, J. (2015) *Guide to Research Techniques in Neuroscience*. Elsevier. Available at: https://doi.org/10.1016/C2013-0-06868-5.

Cooper, G.M. (2019) *The Cell A Molecular Approach*. New York.

Dang, C. V. (2012) 'MYC on the path to cancer', *Cell*. Elsevier B.V., pp. 22–35. Available at: https://doi.org/10.1016/j.cell.2012.03.003.

D'assoro, A.B., Leon-Ferre, R., Braune, E.B. and Lendahl, U. (2022) 'Roles of Notch Signaling in the Tumor Microenvironment', *International Journal of Molecular Sciences*. MDPI. Available at: https://doi.org/10.3390/ijms23116241.

Enomoto, M., Takemoto, D. and Igaki, T. (2021) 'Interaction between Ras and Src clones causes interdependent tumor malignancy via Notch signaling in Drosophila', *Developmental Cell*, 56(15), pp. 2223-2236.e5. Available at: https://doi.org/10.1016/j.devcel.2021.07.002.

Espinosa, L., Cathelin, S., D'Altri, T., Trimarchi, T., Statnikov, A., Guiu, J., Rodilla, V., Ingles-Esteve, J., Nomdedeu, J., Bellosillo, B., Besses, C., Abdel-Wahab, O., Kucine, N., Sun, S.C., Song, G., Mullighan, C.C., Levine, R.L., Rajewsky, K., Aifantis, I. and Bigas, A. (2010) 'The Notch/Hes1 Pathway Sustains NF-κB Activation through CYLD Repression in T Cell Leukemia', *Cancer Cell*, 18(3), pp. 268–281. Available at: https://doi.org/10.1016/j.ccr.2010.08.006.

Fabbri, G., Rasi, S., Rossi, D., Trifonov, V., Khiabanian, H., Ma, J., Grunn, A., Fangazio, M., Capello, D., Monti, S., Cresta, S., Gargiulo, E., Forconi, F., Guarini, A., Arcaini, L., Paulli, M., Laurenti, L., Larocca, L.M., Marasca, R., Gattei, V., Oscier, D., Bertoni, F., Mullighan, C.G., Foa, R., Pasqualucci, L., Rabadan, R., Dalla-Favera, R. and Gaidano, G. (2011) 'Analysis of the chronic lymphocytic leukemia coding

genome: Role of NOTCH1 mutational activation', *Journal of Experimental Medicine*, 208(7), pp. 1389–1401. Available at: https://doi.org/10.1084/jem.20110921.

Ferreira, A. and Aster, J.C. (2022) 'Notch signaling in cancer: Complexity and challenges on the path to clinical translation', *Seminars in Cancer Biology*. Academic Press, pp. 95–106. Available at: https://doi.org/10.1016/j.semcancer.2021.04.008.

Field, A. (2017) *Discovering Statistics Using IBM SPSS Statistics*.

Fischer, A. and Gessler, M. (2007) 'Delta-Notch-and then? Protein interactions and proposed modes of repression by Hes and Hey bHLH factors', *Nucleic Acids Research*. Oxford University Press, pp. 4583–4596. Available at: https://doi.org/10.1093/nar/gkm477.

Fortini, M.E. (2002) 'γ-secretase-mediated proteolysis in cell-surface-receptor signalling', *Nature Reviews Molecular Cell Biology*, pp. 673–684. Available at: https://doi.org/10.1038/nrm910.

Guo, M., Niu, Y., Xie, M., Liu, X. and Li, X. (2023) 'Notch signaling, hypoxia, and cancer', *Frontiers in Oncology*. Frontiers Media S.A. Available at: https://doi.org/10.3389/fonc.2023.1078768.

Guo, Y.J., Pan, W.W., Liu, S.B., Shen, Z.F., Xu, Y. and Hu, L.L. (2020) 'ERK/MAPK signalling pathway and tumorigenesis (Review)', *Experimental and Therapeutic Medicine* [Preprint]. Available at: https://doi.org/10.3892/etm.2020.8454.

https://www.genenames.org/ (no date).

https://www.gsea-msigdb.org/gsea/doc/GSEAUserGuideFrame.html (no date).

https://www.gsea-msigdb.org/gsea/msigdb (no date).

https://www.ncbi.nlm.nih.gov/gene/ (no date).

Hurlbut, G.D., Kankel, M.W. and Artavanis-Tsakonas, S. (2009) 'Nodal points and complexity of Notch-Ras signal integration', *Proceedings of the National Academy of Sciences*, 106(7), pp. 2218–2223. Available at: https://doi.org/10.1073/pnas.0812024106.

Hurtado, C., Safarova, A., Smith, M., Chung, R., Bruyneel, A.A.N., Gomez-Galeno, J., Oswald, F., Larson, C.J., Cashman, J.R., Ruiz-Lozano, P., Janiak, P., Suzuki, T. and Mercola, M. (2019) 'Disruption of NOTCH signaling by a small molecule inhibitor of the transcription factor RBPJ', *Scientific Reports*, 9(1). Available at: https://doi.org/10.1038/s41598-019-46948-5.

Jarriault, S., Brou, C., Logeat, F., Schroeter, E.H., Kopan, R. and Israel, A. (1995) 'Signalling downstream of activated mammalian Notch', *Nature*, 377(6547), pp. 355–358. Available at: https://doi.org/10.1038/377355a0.

Jing, X., Yang, F., Shao, C., Wei, K., Xie, M., Shen, H. and Shu, Y. (2019) 'Role of hypoxia in cancer therapy by regulating the tumor microenvironment', *Molecular Cancer*. BioMed Central Ltd. Available at: https://doi.org/10.1186/s12943-019-1089-9.

Joshi, I., Minter, L.M., Telfer, J., Demarest, R.M., Capobianco, A.J., Aster, J.C., Sicinski, P., Fauq, A., Golde, T.E. and Osborne, B.A. (2009) 'Notch signaling mediates G1/S cell-cycle progression in T cells via cyclin D3 and its dependent kinases', *Blood*, 113(8), pp. 1689–1698. Available at: https://doi.org/10.1182/blood-2008-03-147967.

Kim, M., Cha, G.H., Kim, S., Lee, J.H., Park, J., Koh, H., Choi, K.Y. and Chung, J. (2004) ' MKP-3 Has Essential Roles as a Negative Regulator of the Ras/Mitogen-Activated Protein Kinase Pathway during Drosophila Development ', *Molecular and Cellular Biology*, 24(2), pp. 573–583. Available at: https://doi.org/10.1128/mcb.24.2.573-583.2004.

De la Pompa, J.L. and Epstein, J.A. (2012) 'Coordinating Tissue Interactions: Notch Signaling in Cardiac Development and Disease', *Developmental Cell*, pp. 244–254. Available at: https://doi.org/10.1016/j.devcel.2012.01.014.

Lambris, J.D. (2018) *Molecular Mechanisms of Notch Signaling*. Edited by T. Borggrefe and B.D. Giaimo. Cham: Springer International Publishing (Advances in Experimental Medicine and Biology). Available at: https://doi.org/10.1007/978-3-319-89512-3.

Lee, S.Y., Kumano, K., Nakazaki, K., Sanada, M., Matsumoto, A., Yamamoto, G., Nannya, Y., Suzuki, R., Ota, S., Ota, Y., Izutsu, K., Sakata-Yanagimoto, M., Hangaishi, A., Yagita, H., Fukayama, M., Seto, M., Kurokawa, M., Ogawa, S. and Chiba, S. (2009) 'Gain-of-function mutations and copy number increases of Notch2 in diffuse large B-cell lymphoma', *Cancer Science*, 100(5), pp. 920–926. Available at: https://doi.org/10.1111/j.1349-7006.2009.01130.x.

Lehal, R., Zaric, J., Vigolo, M., Urech, C., Frismantas, V., Zangger, N., Cao, L., Berger, A., Chicote, I., Loubery, S., Choi, S.H., Koch, U., Blacklow, S.C., Palmer, H.G., Bornhauser, B., Gonzalez-Gaitan, M., Arsenijevic, Y., Zoete, V., Aster, J.C., Bourquin, J.P. and Radtke, F. (2020) 'Pharmacological disruption of the Notch transcription factor complex', *Proceedings of the National Academy of Sciences*, 117(28), pp. 16292–16301. Available at: https://doi.org/10.1073/pnas.1922606117.

Love, M., Anders, S. and Huber, W. (2014) 'Beginner's guide to using the DESeq2 package'. Available at: https://doi.org/10.1101/002832.

Love, M.I., Huber, W. and Anders, S. (2014) 'Moderated estimation of fold change and dispersion for RNA-seq data with DESeq2', *Genome Biology*, 15(12). Available at: https://doi.org/10.1186/s13059-014-0550-8.

Luo, J.E. and Li, Y.M. (2022) 'Turning the tide on Alzheimer's disease: modulation of γ-secretase', *Cell and Bioscience*. BioMed Central Ltd. Available at: https://doi.org/10.1186/s13578-021-00738-7.

Majumder, S., Crabtree, J.S., Golde, T.E., Minter, L.M., Osborne, B.A. and Miele, L. (2021) 'Targeting Notch in oncology: the path forward', *Nature Reviews Drug Discovery*. Nature Research, pp. 125–144. Available at: https://doi.org/10.1038/s41573-020-00091-3.

Mašek, J. and Andersson, E.R. (2017) 'The developmental biology of genetic notch disorders', *Development (Cambridge)*. Company of Biologists Ltd, pp. 1743–1763. Available at: https://doi.org/10.1242/dev.148007.

Mitchell, S., Vargas, J. and Hoffmann, A. (2016) 'Signaling via the NFκB system', *Wiley Interdisciplinary Reviews: Systems Biology and Medicine*. Wiley-Blackwell, pp. 227–241. Available at: https://doi.org/10.1002/wsbm.1331.

Moellering, R.E., Cornejo, M., Davis, T.N., Bianco, C.D., Aster, J.C., Blacklow, S.C., Kung, A.L., Gilliland, D.G., Verdine, G. and Bradner, J.E. (2009) 'Direct inhibition of the NOTCH transcription factor complex', *Nature*, 462(7270), pp. 182–188. Available at: https://doi.org/10.1038/nature08543.

Mukherjee, M., Fogarty, E., Janga, M. and Surendran, K. (2019) 'Notch signaling in kidney development, maintenance, and disease', *Biomolecules*. MDPI AG. Available at: https://doi.org/10.3390/biom9110692.

Oeckinghaus, A., Hayden, M.S. and Ghosh, S. (2011) 'Crosstalk in NF-κB signaling pathways', *Nature Immunology*, pp. 695–708. Available at: https://doi.org/10.1038/ni.2065.

Osipo, C., Golde, T.E., Osborne, B.A. and Miele, L.A. (2008) 'Off the beaten pathway: The complex cross talk between Notch and NF-κB', *Laboratory Investigation*, pp. 11–17. Available at: https://doi.org/10.1038/labinvest.3700700.

Oswald, F., Kostezka, U., Astrahantseff, K., Bourteele, S., Dillinger, K., Zechner, U., Ludwig, L., Wilda, M., Hameister, H., Knochel, W., Liptay, S. and Schmid, R.M. (2002) 'SHARP is a novel component of the

Notch/RBP-Jκ signalling pathway', *EMBO Journal*, 21(20), pp. 5417–5426. Available at: https://doi.org/10.1093/emboj/cdf549.

Palomero, T., Lim, W.K., Odom, D.T., Sulis, M.L., Real, P.J., Margolin, A., Barnes, K.C., O'Neil, J., Neuberg, D., Weng, A.P., Aster, J.C., Sigaux, F., Solier, J., Look, A.T., Young, R.A., Califano, A. and Ferrando, A.A. (2006) 'NOTCH1 directly regulates *c-MYC* and activates a feed-forward-loop transcriptional network promoting leukemic cell growth', *Proceedings of the National Academy of Sciences*, 103(48), pp. 18261–18266. Available at: https://doi.org/10.1073/pnas.0606108103.

Porta, C., Paglino, C. and Mosca, A. (2014) 'Targeting PI3K/Akt/mTOR signaling in cancer', *Frontiers in Oncology*. Frontiers Research Foundation. Available at: https://doi.org/10.3389/fonc.2014.00064.

Promega, C. (2015) *Dual-Luciferase ® Reporter Assay System Instructions for use of Products E1910 and E1960*. Available at: www.promega.com.

Promega Corporation (Instructions for use of Products E1910 and E1960) (2015) *Dual-Luciferase ® Reporter Assay System Instructions for use of Products E1910 and E1960*. Available at: www.promega.com.

Rampias, T., Vgenopoulou, P., Avgeris, M., Polyzos, A., Stravodimos, K., Valavanis, C., Scorilas, A. and Klinakis, A. (2014) 'A new tumor suppressor role for the Notch pathway in bladder cancer', *Nature Medicine*, 20(10), pp. 1199–1205. Available at: https://doi.org/10.1038/nm.3678.

Reichrath, J. and Reichrath, S. (2021) *Notch Signaling in Embryology and Cancer*. Edited by J. Reichrath and S. Reichrath. Cham: Springer International Publishing (Advances in Experimental Medicine and Biology). Available at: https://doi.org/10.1007/978-3-030-55031-8.

Reimand, J., Isserlin, R., Voisin, V., Kucera, M., Tannus-Lopes, C., Rostamianfar, A., Wadi, L., Meyer, M., Wong, J., Xu, C., Merico, D. and Bader, G.D. (2019) 'Pathway enrichment analysis and visualization of omics data using g:Profiler, GSEA, Cytoscape and EnrichmentMap', *Nature Protocols*, 14(2), pp. 482–517. Available at: https://doi.org/10.1038/s41596-018-0103-9.

Ronchini, C. and Capobianco, A.J. (2001) ' Induction of Cyclin D1 Transcription and CDK2 Activity by Notch ic : Implication for Cell Cycle Disruption in Transformation by Notch ic ', *Molecular and Cellular Biology*, 21(17), pp. 5925–5934. Available at: https://doi.org/10.1128/mcb.21.17.5925-5934.2001.

Rudack, T., Xia, F., Schlitter, J., Kotting, C. and Gerwert, K. (2012) 'Ras and GTPase-activating protein (GAP) drive GTP into a precatalytic state as revealed by combining FTIR and biomolecular simulations',

BIOPHYSICS AND COMPUTATIONAL BIOLOGY, 109(38), pp. 15295–15300. Available at: https://doi.org/10.1073/pnas.1204333109/-/DCSupplemental.

Sanchez-Martin, M. and Ferrando, A. (2017) 'The NOTCH1-MYC highway toward T-cell acute lymphoblastic leukemia', *Blood*, 129(9), pp. 1124–1133. Available at: https://doi.org/10.1182/blood-2016-09-692582.

Shimobayashi, M. and Hall, M.N. (2014) 'Making new contacts: The mTOR network in metabolism and signalling crosstalk', *Nature Reviews Molecular Cell Biology*, 15(3), pp. 155–162. Available at: https://doi.org/10.1038/nrm3757.

Smale, S.T. (2010) 'Luciferase Assay', *Cold Spring Harbor Protocols*, 2010(5), p. pdb.prot5421. Available at: https://doi.org/10.1101/pdb.prot5421.

Song, L.L., Peng, Y., Rizzo, P., Chaturvedi, V., Weijzen, S., Kast, W.M., Stone, P.J.B., Santos, L., Loredo, A., Lendahl, U., Sonenshein, G., Osborne, B., Qin, J.Z., Pannuti, A., Nickoloff, B.J. and Miele, L. (2008) 'Notch-1 associates with IKKα and regulates IKK activity in cervical cancer cells', *Oncogene*, 27(44), pp. 5833–5844. Available at: https://doi.org/10.1038/onc.2008.190.

Subramanian, A., Tamayo, P., Mootha, V.K., Mukherjee, S., Ebert, B.L., Gillette, M.A., Paulovich, A., Pomeroy, S.L., Golub, T.R., Lander, E.S. and Mesirov, J.P. (2005) 'Gene set enrichment analysis: A knowledge-based approach for interpreting genome-wide expression profiles', *Proceedings of the National Academy of Sciences*, 102(43), pp. 15545–15550. Available at: https://doi.org/10.1073/pnas.0506580102.

The Cancer Genome Atlas Research Network (2015) 'Comprehensive, Integrative Genomic Analysis of Diffuse Lower-Grade Gliomas', *New England Journal of Medicine*, 372(26), pp. 2481–2498. Available at: https://doi.org/10.1056/NEJMoa1402121.

Wagner, V.P., Ferrarotto, R., Vargas, P.A., Martins, M.D., Bingle, C.D. and Bingle, L. (2023) 'Drug-based therapy for advanced adenoid cystic carcinoma: Current landscape and challenges based on an overview of registered clinical trials', *Critical Reviews in Oncology/Hematology*. Elsevier Ireland Ltd. Available at: https://doi.org/10.1016/j.critrevonc.2022.103886.

Wang, J., Qin, H., Liang, J., Zhu, Y., Lian, L., Zheng, M. and Han, H. (2007) 'The Transcriptional Repression Activity of KyoT2 on the Notch/RBP-J Pathway Is Regulated by PIAS1-catalyzed SUMOylation', *Journal of Molecular Biology*, 370(1), pp. 27–38. Available at: https://doi.org/10.1016/j.jmb.2007.04.010.

Wang, N.J., Sanborn, Z., Arnett, K.L., Bayston, L.J., Liao, W., Proby, C.M., Leigh, I.M., Collisson, E.A., Gordon, P.B., Jakkula, L., Pennypacker, S., Zou, Y., Sharma, M., North, J.P., Vemula, S.S., Mauro, T.M., Neuhaus, I.M., LeBoit, P.E., Hur, J.S., Park, K., Huh, N., Kwok, P.Y., Arron, S.T., Massion, P.P., Bale, A.E., Hussler, D., Cleaver, J.E., Gray, J.W., Spellman, P.T., South, A.P., Aster, J.C., Blacklow, S.C. and Cho, R.J. (2011) 'Loss-of-function mutations in Notch receptors in cutaneous and lung squamous cell carcinoma', *Proceedings of the National Academy of Sciences of the United States of America*, 108(43), pp. 17761–17766. Available at: https://doi.org/10.1073/pnas.1114669108.

Weng, A.P., Ferrando, A.A., Lee, W., Morris, J.P., Silverman, L.B., Sanchez-Irizarry, C., Blacklow, S.C., Look, A.T. and Aster, J.C. (2004) 'Activating mutations of NOTCH1 in human T cell acute lymphoblastic leukemia', *Science*, 306(5694), pp. 269–271. Available at: https://doi.org/10.1126/science.1102160.

Weng, A.P., Millholland, J.M., Yashiro-Ohtani, Y., Arcangeli, M.L., Lau, A., Wai, C., del Bianco, C., Rodrigez, C.G., Sai, H., Tobias, J., Li, Y., Wolfe, M.S., Shachaf, C., Felsher, D., Blacklow, S.C., Pear, W.S. and Aster, J.C. (2006) 'c-Myc is an important direct target of Notch1 in T-cell acute lymphoblastic leukemia/lymphoma', *Genes and Development*, 20(15), pp. 2096–2109. Available at: https://doi.org/10.1101/gad.1450406.

Wielockx, B., Grinenko, T., Mirtschink, P. and Chavakis, T. (2019) 'Hypoxia pathway proteins in normal and malignant hematopoiesis', *Cells*. MDPI. Available at: https://doi.org/10.3390/cells8020155.

Wolf, D., Smylla, T.K., Reichmuth, J., Hoffmeister, P., Kober, L., Zimmermann, M., Turkiewicz, A., Borgreffe, T., Nagel, A.C., Oswald, F., Preiss, A. and Maier, D. (2019) 'Nucleo-cytoplasmic shuttling of Drosophila Hairless/Su(H) heterodimer as a means of regulating Notch dependent transcription', *Biochimica et Biophysica Acta - Molecular Cell Research*, 1866(10), pp. 1520–1532. Available at: https://doi.org/10.1016/j.bbamcr.2019.07.008.

Wu, L., Aster, J.C., Blacklow, S.C., Lake, R., Artavanis-Tsakonas, S. and Griffin, J.D. (2000) 'MAML1, a human homologue of Drosophila Mastermind, is a transcriptional co-activator for NOTCH receptors', *Nature Genetics*, 26(4), pp. 484–489. Available at: https://doi.org/10.1038/82644.

Zhou, B., Lin, W., Long, Y., Yang, Y., Zhang, H., Wu, K. and Chu, Q. (2022) 'Notch signaling pathway: architecture, disease, and therapeutics', *Signal Transduction and Targeted Therapy*. Springer Nature. Available at: https://doi.org/10.1038/s41392-022-00934-y.

Zou, Z., Tao, T., Li, H. and Zhu, X. (2020) 'MTOR signaling pathway and mTOR inhibitors in cancer: Progress and challenges', *Cell and Bioscience*. BioMed Central Ltd. Available at: https://doi.org/10.1186/s13578-020-00396-1.

9. Resume

I was born in 1996 in north-western part of Croatia where I attended the high school with a track in natural sciences and mathematics. I graduated from the high school with triple science (biology, chemistry and physics), mathematics and advanced level English language diploma in 2015. In the same year, I went on to study for Bachelor's degree in Biology at the University of Zagreb which I completed with highest honor in 2018. During the senior year of my bachelor's studies, I was awarded a Dean's award for the best student of the study program. Starting from 2018, I got enrolled in the Master's program in Experimental Biology with major in Physiology and Immunobiology at the same university. In 2019, I was pronounced the exceptionally successful student by Biology Department Board. Moreover, I was also granted a study place at the University of Western Australia in Perth for a Master of Biomedical Science with specialization in Biochemistry and Molecular Biology which I unfortunately had to decline due to financial reasons. Nevertheless, in the same year, I simultaneously pursued the study for Master of Science in Biology degree at Ulm University in Germany where I chose Endocrinology and Behavioral Physiology as my majors and Virology as a minor track.

Throughout my studies, I completed five internships. The first two were at Ruder Boskovic Institute in Zagreb in the Laboratory for Inorganic Environmental Geochemistry and Chemodynamics of Nanoparticles under the supervision of Dr. Zeljka Fiket. My work consisted of sample preparations for multielement analysis and experiments related to metal adsorption on geopolymer matrices. The third internship was also at Ruder Boskovic Institute but in a Laboratory for Epigenomics under the supervision of Dr. Koraljka Gall Troselj. I was tasked with conducting various cellular and molecular biology techniques ranging from DNA and RNA isolation, PCR and qRT-PCR to western blot, and flow cytometry. The fourth internship was at the University Medical Center Ulm at the Institute of Molecular Virology under Dr. Konstantin Sparrer's supervision where the main topic was the interplay between innate immunity and viruses. I carried out molecular cloning, autophagy assay and flow cytometry methods. Finally, the fifth internship was prior to my thesis research in Prof. Dr. Franz Oswald's research group at Internal Medicine I Department as a part of the University Medical Center Ulm. My work comprised cell culture (HeLa, HEK 293, and AML cell lines), calcium chloride, and lipofectamine 2000 transfection, plasmid Maxi Prep, agarose gel electrophoresis, co-immunoprecipitation, NucleoCounter NC3000 viability, and fixed cell-cycle assay, flow cytometry, cytospin followed by May-Grunwald-Giemsa staining, immunofluorescence, single reporter Firefly and dual reporter (Firefly and Renilla) luciferase assay system.

During my studies I was awarded a total of 5 scholarships. I received the academic excellence scholarship from my hometown, and from my home county, as well as STEM scholarship from the Croatian

Government. In 2019, I was awarded Deutschlandstipendium (German Scholarship) from the German Federal Ministry of Education and Research. In the following year, I also got selected for DAAD scholarship from Deutscher Akademischer Austauschdienst (German Academic Exchange Service).

Last but not least, my spare time activities and hobbies include swimming, hiking, cultural travel and crypto-trading. I also very much enjoy hanging out with my friends and debating various topics from a philosophical point of view.